



Characterising patterns of heavy precipitation events in the eastern Mediterranean using a weather radar and convection-permitting WRF simulations

Moshe Armon¹, Francesco Marra¹, Yehouda Enzel¹, Dorita Rostkier-Edelstein², Efrat Morin¹

5 ¹Fredy and Nadine Herrmann Institute of Earth Sciences, the Hebrew University of Jerusalem, Edmond J. Safra Campus, Jerusalem, 9190401, Israel

² Department of Applied Mathematics, Environmental Sciences Division, IIBR, Ness-Ziona, 7410001, Israel

Correspondence to: Moshe Armon (moshe.armon@mail.huji.ac.il)

Abstract. Heavy precipitation events (HPEs) can lead to natural hazards (floods, debris flows) and contribute to water resources. Rainfall patterns govern HPEs effects. Thus, a correct characterisation and prediction of rainfall patterns is crucial for coping with HPEs. Information from rain gauges is generally limited due to the sparseness of the networks, especially in presence of sharp climatic gradients. Forecasting HPEs depends on the ability of weather models to generate credible rainfall patterns. This paper characterises rainfall patterns during HPEs based on high-resolution weather radar data and evaluates the performance of a high-resolution, convection-permitting, Weather Research and Forecasting (WRF) model in simulating these patterns. We identified 41 HPEs in the eastern Mediterranean from a 24-year radar record using local thresholds based on quantiles for different durations, and we ran model simulations of these events. For most durations, HPEs near the coastline are characterised by the highest rain intensities, however, for short durations, the highest rain intensities characterise the inland desert. During the rainy season, the centre-of-mass of the rain field progresses from the sea inland. Rainfall during HPEs is highly localised both in space (<10 km decorrelation distance) and in time (<5 min). WRF model simulations were accurate in generating the structure and location of the rain fields in 39 out of 41 HPEs. However, they showed a positive bias with respect to the radar estimates and exhibited errors in the spatial location of the heaviest precipitation. Our results indicate that convection-permitting model outputs can provide reliable climatological analyses of heavy precipitation patterns; conversely, flood forecasting requires the use of ensemble simulations to overcome the spatial location errors.

1 Introduction

25 Heavy precipitation events (HPEs) cause natural hazards such as flash, riverine, and urban floods, landslides and debris flows; at the same time, they also serve as a resource in recharging ground and surface water reservoirs (e.g., Bogaard and Greco, 2016; Borga et al., 2014; Borga and Morin, 2014; Doswell et al., 1996; Nasta et al., 2018; Raveh-Rubin and Wernli, 2015; Samuels et al., 2009; Taylor et al., 2013; UN-Habitat, 2011). Diverse rainfall patterns during HPEs cause different hydrological responses, thus an accurate representation of rainfall patterns during HPEs is crucial in detecting and predicting climate-change induced precipitation changes (Maraun et al., 2010; Trenberth et al., 2003). In particular, understanding the specific interactions

30



between rainstorms and catchments is critical in small watersheds, where accurate, high spatiotemporal resolution observations and forecasts are required (e.g., Blöschl and Sivapalan, 1995; Cristiano et al., 2017). However, these data may not be available through operational tools, such as rain gauge networks and coarse scale weather models (e.g., commonly used, global or even regional circulation models). High-resolution observation and HPE forecasts remain thus a challenge (Borga et al., 2011; 35 Collier, 2007; Doswell et al., 1996).

Rain gauge data can be used to quantify general characteristics of HPEs (such as rain intensity and depth at the point scale), but, their density is generally insufficient to adequately represent the spatial gradients, particularly in case of sparsely gauged regions, short duration events, and arid climates (Amponsah et al., 2018; Kidd et al., 2017; Morin et al., 2009, 2019). This problem is enhanced in regions characterised by high climatic gradients such as the eastern Mediterranean (EM) (El-Samra et al., 2017; Marra et al., 2017; Marra and Morin, 2015; Morin and Gabella, 2007; Rostkier-Edelstein et al., 2014). Thus, 40 characterising HPEs with high resolution in such regions must be supported by other types of records. Remotely-sensed precipitation estimates, such as those acquired from weather radars, provide the necessary spatiotemporal resolutions (e.g., 1 km, 5 min) and coverage (regional scale), and have been shown to be useful for analysing specific events (e.g., Borga et al., 2007; Dayan et al., 2001; Krichak et al., 2000; Smith et al., 2001). Where continuous radar records exist, they have been used 45 in climatological studies as well (Belachsen et al., 2017; Bližňák et al., 2018; Peleg et al., 2012; Saltikoff et al., 2019; Smith et al., 2012). However, climatological characterisations of rainfall patterns during HPEs are rare in literature and often based on rain gauge identification of HPEs (Panziera et al., 2018; Thorndahl et al., 2014).

High-resolution numerical weather predictions (NWP) allow to simulate and forecast HPEs, and represent an added value for understanding their past and present patterns, and predicting possible future behaviours (Cassola et al., 2015; Deng et al., 2015; 50 El-Samra et al., 2017; Kendon et al., 2014; Prein et al., 2015; Rostkier-Edelstein et al., 2014; Yang et al., 2014). In particular, convection-permitting models are increasingly used in weather forecasts, climatological studies and event-based reanalyses (e.g., Ban et al., 2014; Fosser et al., 2014; Hahmann et al., 2010; Khodayar et al., 2016; Prein et al., 2015; Rostkier-edelstein et al., 2015). Such models downscale global or regional NWP models, and allow to directly represent convective rainfall that, due to its high-intensity and local characteristics, often plays a major role in HPEs (e.g., Flaounas et al., 2018). Additionally, 55 they can provide 3D fields of otherwise unmeasurable meteorological variables, thus contributing to our understanding of the dynamics of HPEs. Studies based on high-resolution NWP models commonly focus on specific cases, with only a few also examining the climatology of model results, either for determining the atmospheric conditions that trigger HPEs, or understanding the overall rainfall pattern in comparison with observational records (e.g., Flaounas et al., 2019; Kendon et al., 2014; Khodayar et al., 2018). Commonly, climate change studies based on high-resolution NWP models characterise the 60 expected changes in precipitation focusing on rainfall intensity or frequency, or some derived index (e.g., Ban et al., 2014; Hochman et al., 2018a; Schär et al., 2016; Westra et al., 2014).

A basic question, however, remains unanswered: Is the model description of rainfall during HPEs credible? To answer this question, both a realistic spatiotemporal representation of rainfall during HPEs and a large number of observed HPEs are necessary. In this paper, we present a successful step in this direction based on a corrected and calibrated, 24-year long record



65 of weather radar data recently developed for the EM, and found to adequately represent extreme precipitation events (Marra
and Morin, 2015). As an essential step in understanding and quantifying rainfall-generating processes involved in HPEs, and
as a basis for a future study that includes downscaling of climate change projections to understand changes in rainfall patterns,
we aim here to (a) systematically characterise high-resolution rainfall patterns during HPEs in the hydroclimatically-
heterogeneous EM, and (b) assess the capabilities of a regional convection-permitting weather model to simulate these patterns.
70 To do so we identified 41 HPEs embedded in the radar record, and simulated them using a convection-permitting weather
research and forecasting (WRF) model (Skamarock et al., 2008). Then, we quantified several rainfall characteristics, and
compared simulated rain fields to radar estimates to evaluate the ability of the model to reproduce the rainfall patterns.
Section 2 describes the study region. The radar and the weather model data are explained in Sect. 3.1-3.2. Identification and
synoptic classification of HPEs are presented in Sect. 3.3 and Sect. 3.4, respectively. The methods used in evaluating model
75 performance is in Sect. 3.5. Section 4 presents the results of the evaluation and characterisation of rainfall patterns during
HPEs. Section 5 provides a discussion and a summary of the study.

2 Study region

This study focuses on the EM region, where Mediterranean climate (with parts of it getting a mean annual precipitation >1000
mm year⁻¹) drops to hyperarid (<50 mm year⁻¹) over a short distance (Goldreich, 2012) (Fig. 1). Precipitation is dominated by
80 rainfall, and occurs mainly between October and May, with summer months (June-September) being essentially dry (Kushnir
et al., 2017). Most of this rainfall is associated to cold north-westerly flows at the rear part of Mediterranean Cyclones (MCs).
These MCs pass above the warm water of the Mediterranean Sea, absorbing moisture and precipitating it over the EM region
(Alpert et al., 2004; Alpert and Shay-EL, 1994; Armon et al., 2019; Saaroni et al., 2010; Ziv et al., 2015). High surface water
temperature favours high intensity rainfall and floods, most commonly at the beginning of the rainy season and near the sea.
85 While MCs move inland and towards the desert, a substantial amount of the moisture is lost, and rainfall occurrence and
amounts are greatly reduced (Enzel et al., 2008). In this arid region HPEs are associated not only to MCs (Armon et al., 2018;
Kahana et al., 2002), but also to the Active Red Sea Trough (ARST) (Ashbel, 1938; Krichak et al., 1997; De Vries et al., 2013)
and, more rarely, to Tropical Plumes (Armon et al., 2018; Rubin et al., 2007; Tubi et al., 2017). Commonly, rainfall during
ARSTs is of spotty nature, could reach far into the desert, and could have very high intensities (Armon et al., 2018; Sharon,
90 1972). Conversely, during Tropical Plumes, rainfall is widespread and can simultaneously cover most of the region with
moderate intensities. Desert HPEs frequently result in large and sometimes devastating flash floods (e.g., Armon et al., 2018;
Dayan and Morin, 2006; Farhan and Anbar, 2014; Kahana et al., 2002; Saaroni et al., 2014; Seager et al., 2014).
Projections for precipitation in the EM indicate a substantial decrease in annual rainfall amounts (Giorgi and Lionello, 2008);
however, the importance of credible HPE simulations stems, among others, from opposing trends that may appear between
95 number and intensity of HPEs generated by different synoptic conditions (Alpert et al., 2002; Hochman et al., 2018a, 2019;



Marra et al., 2019); for example, based on Dead Sea sedimentologic data, it was suggested that when MCs frequency is reduced, i.e., a regional drought, the frequency of HPEs generated by ARST may increase (Ahlborn et al., 2018).

3 Methodology and data

3.1 Weather radar data

100 The weather radar data used in this study consist of 24 hydrological years (September-August) between 1990-1991 and 2013-
2014 observed by the Electrical Mechanical Services (EMS/Shacham) C-band weather radar, located at Ben-Gurion Airport
(Fig. 1). Radar quantitative precipitation estimates (QPE) were produced by applying physically based corrections and gauge-
based adjustment procedures (see details in Marra and Morin, 2015), and were available at 1 km², ~5-min resolutions.
Examining the radar QPE and comparing it with rain gauges at hourly and yearly resolution yielded a root mean square error of
105 1.4-3.2 mm h⁻¹ and 13-220 mm y⁻¹, respectively, and a bias of 0.8-1.1 (hourly) and 0.9-1.1 (yearly) (Marra and Morin, 2015).
This archive was previously used for a series of studies focusing on high intensity precipitation, such as precipitation frequency
analysis (Marra et al., 2017; Marra and Morin, 2015), floods (Rinat et al., 2018; Zoccatelli et al., 2019), and characterisation
of convective rain cells (Belachsen et al., 2017; Peleg et al., 2018). Few issues potentially affecting the QPE should be
mentioned. The radar was turned off during the dry season and, for technical reasons, sometimes during the wet season; thus,
110 a few severe storms were missed and are not included in the archive. There is a long-term decline in the availability and quality
of the radar data that might have decreased the number of high quality archived HPEs during the years, mainly since 2010.
Since we do not aim at providing a *complete* climatology, these aspects are not expected to influence the results of the study.
Due to technical reasons, the radar products were not always available at their intended temporal resolution (~5 min) and
longer gaps may exist between consecutive radar scans. Gaps of <20 min between consecutive radar scans were linearly
115 interpolated to recreate the 5-min resolution; gaps of >20 min were treated as missing data. Due to the uneven spatial
distribution of rain gauges, adjustment procedures may inadequately represent the south-easternmost areas covered by the
radar, where gauge network is the sparsest. Finally, due to overshooting of the radar beam, precipitation occurring east of the
Dead Sea (Fig. 1) is generally underestimated.

3.2 WRF model configuration

120 The WRF model was configured using three, 1-way nested domains, at a 1:5 resolution ratio between them (Fig. 1). The inner
domain (551X551 pixels) is set at a 1 km² horizontal resolution, to be comparable with the radar data. To comply with Courant-
Friedrichs-Lewy numerical stability criterion, model time steps at the innermost domain are 4-8 seconds (Warner, 2011),
however, to spare computer storage, outputs were saved at 10 min intervals. When analysed, the WRF grid was interpolated
from a Lambert projection grid to a similar size grid on Transverse Mercator projection, as in the radar archive. It is important
125 to note that a 1 km² spatial resolution enables to explicitly resolve convection, without the use of parametrisation (e.g., Prein
et al., 2015). The model input data are six-hourly ERA-Interim reanalyses, at ~80 km horizontal resolution and with 60 vertical



levels, including sea surface temperature, along with basic meteorological parameters (Dee et al., 2011). The model was used to simulate the HPEs identified in the radar archive (Sect 3.2). Each simulation started 24 h prior to the beginning of the event, rounded down to the previous 6 h, and ended with the HPE ending, rounded up to the next 6 h. Therefore, the spin-up period of each simulation is at least 24 h. Other model settings, presented in Table 1, were selected because they are considered suitable for convection-permitting simulations (e.g., Romine et al., 2013; Schwartz et al., 2015).

3.3 HPEs identification

HPEs have various definitions in different research fields and geographical regions. For example, climatologically, HPEs are commonly associated to a specific time interval (i.e. sub-daily to a number of consecutive days) during which precipitation depth surpasses a threshold representing a predefined quantile (e.g., 95th or 99th), or high, but constant, intensity (e.g., 10, 20, or 50 mm day⁻¹) (e.g., Drobinski et al., 2014; Nuissier et al., 2011; Westra et al., 2014; Zhang et al., 2011b). On the other hand, hydrological definitions usually focus on the resulting flood. In general, a good definition of HPE should also include the areal dimension, in order to consider hydrological and social impacts (Easterling et al., 2000).

Here we define HPEs by the exceedance of local, quantile-based thresholds over a sufficiently large area. The decision to set local thresholds is due to the sharp climatic gradient characterising the study area. To decrease the computational efforts and guarantee adequate temporal sampling, the HPE identification was based on a radar database comprising the hourly intervals in which at least 60% of the expected radar scans are available (Marra et al., 2017). For a set of durations between 1 and 72 hours we defined the threshold as the 99.5th quantile of the non-zero (i.e. >0.1 mm) hourly amounts observed in each radar pixel. Depending on duration and location, these are equivalent to annual return periods of roughly 2-10 years (Fig. 2). To account for the spatial scale, we classify as HPEs all time intervals during which at least 1000 pixels (i.e., 1000 km²) exceeded their local threshold. Jointly, these thresholds (99.5% for each pixel, and aggregation of 1000 pixels for an event) settle the trade-off between having too many (or too few) events and accounting for HPEs that are too local (or only including the most widespread rainstorms). These selected thresholds allow to analyse a reasonable number of diverse HPEs, with some HPEs being quite local and others more widespread.

The selection procedure yielded 76-98 individual events for each of the examined durations, summing up to 120 when overlaps between durations are included. Similar to Marra and Morin (2015), storms were separated by at least 24 hours with <100 pixels displaying rainfall >0.1 mm. Since the ERA-Interim data are available on a 6 h resolution, too short rainstorms (<12 h) were excluded from the analysis. Storms longer than 144 h were excluded to avoid major changes in sea surface temperature during events. In addition, events were discarded manually when radar data was abundantly contaminated by ground clutter due to anomalous propagation, or in case other data quality issues were observed. The final list of HPEs consists of 41 independent events lasting on average 3.4 ± 1.6 days (Table S1).

For each of these events, a filter was used to remove pixels with residual ground clutter. Pixels in which the probability of rain detection (POD, i.e., the fraction of time in which the pixel exceeds 0.1 mm h⁻¹) exceeds 10% and is larger than 1.9 times the average POD of the surrounding area (25 × 25 km) were removed. The extent of the explored area and of the ratio were



160 subjectively chosen after examining ranges between 1-3 (for the ratio) and 5-50 km (for the areal extent). Additional areas
known to be persistently contaminated by ground echoes (from our experience and earlier studies) were masked out manually
(e.g., the circular area near the radar). Together, these procedures excluded ~0.5% of the radar pixels.

3.4 Synoptic classification

We classified the HPEs into two classes representing the most common rainy synoptic circulation patterns prevailing in the
165 region: MC and ARST. To do so, we rely on the semi-objective synoptic classification by Alpert et al. (2004), based on
meteorological fields at the 1000 hPa pressure level. We classified a HPE as MC if one of the following conditions occurred:
(1) the majority of the days comprising the HPE were considered according to Alpert et al. (2004) as days with either a MC or
a high-pressure system following a MC; (2) one of the days during the HPE was a MC and none of them was an ARST.
Similarly, we classified a HPE as an ARST if (1) the majority of its days were classified as ARST according to Alpert et al.
170 (2004), or (2) one of its days was an ARST and none of them was a MC. The abovementioned TP synoptic pattern (Rubin et
al., 2007; Tubi et al., 2017) is not a part of our classification because of the low frequency and because they do not appear in
a near sea level pressure meteorological fields. Specifically, one HPE (#41; Table S1) was characterised, during its 5-day
duration, first by the prevalence of TP (Armon et al., 2018) and then by MC; it was classified here as a MC. Despite the
simplification, these two classes were recently shown to exhibit distinct characteristics of the rainfall intensity distribution
175 (Marra et al., 2019). Indeed, 85% and 15% of HPEs were classified as MCs and ARSTs, respectively (Table S1), reasonably
following the expected proportions of the two synoptic circulation patterns (Goldreich et al., 2004; Saaroni et al., 2010).

3.5 Evaluation of simulated rain fields

Inaccurate initial conditions in presence of non-linear precipitation generation processes, together with the presence of
atmospheric instabilities, may limit the atmospheric predictability and, consequently, the modelling skills (Anthes et al., 1985).
180 Moreover, increasing the model resolution may pose difficulties in a pixel-by-pixel evaluation of the forecasts (e.g., Davis et
al., 2006; Mass et al., 2002). Approaches more suitable for high-resolution rainfall fields range from simple visual comparisons
to more sophisticated, object-oriented or filtering methods capable of representing spatiotemporal properties of the fields (e.g.,
Davis et al., 2006; Gilleland et al., 2009; Roberts and Lean, 2008). In this study, we applied visual comparisons and several
numerical measures for comparing the radar-observed QPE with the WRF-derived rain field.

185 3.5.1 Fractions skill score

To evaluate rainfall accumulation at different neighbourhood sizes (namely, spatial scales), we use the method suggested by
Roberts and Lean (2008). The methodology includes a conversion of the continuous rain field to a binary field based on the
exceedance of a given rain depth threshold. The fraction of model-output positive pixels (i.e. pixels that have exceeded the
threshold) within a certain neighbourhood size is then compared with the matching fraction from the radar-QPE, through the
190 fractions skill score (FSS) statistic (Supplementary material [S1]). When the forecast is perfect and unbiased, i.e., when an



equal number of observed (in our case, radar) and forecasted (WRF) pixels exceed the threshold, the FSS=1. If there is a bias, the FSS would tend asymptotically to a lower value. To quantitatively evaluate the model's ability to predict the observed rainfall above the selected threshold, within a close-enough distance, the uniform FSS (halfway between a random forecast and a perfect skill forecast, yielding a hit rate of 0.5; [S1]) is also calculated. FSS score larger than the uniform FSS is considered skilful. It is important to note that if the FSS exceeds the uniform FSS at a spatial scale that is too large, the forecast might still be skilful, but it is not useful. We applied the FSS method to the cumulative rain field, comparing the radar QPE and WRF rainfall output (Sect. 4.1.1).

3.5.2 Structure-amplitude-location (SAL) analysis

To evaluate the characteristics of the WRF precipitation forecasts errors, we used the object-oriented structure-amplitude-location (SAL) analysis (Wernli et al., 2008) (Supplementary material [S2]). As in the FSS analysis, it was applied to the cumulative rain field. The SAL analysis splits the rain field into three distinct components and yields a skill score for the forecast of each of them; in each of the components, zero score indicates a perfect forecast. The amplitude component (A) expresses the model over/underestimation of the total rainfall for a specific rainstorm (with $A \in [-2,2]$, and $A = 1$ or $A = -1$ indicating over and underestimation by a factor of 3, respectively). The location component ($L \in [0,2]$) sums the differences between modelled and observed (a) centre of mass of precipitation and (b) average distance between the centre of mass and the location of precipitation objects that constitute the rain field (i.e., connected regions in which the cumulative rainfall exceeds 1/15 of the maximal cumulated value; Wernli et al., 2008). The structure component ($S \in [-2,2]$) quantifies the tendency of the forecasted precipitation objects to be either too smooth (positive values) or too noisy (negative values) with respect to the observations.

3.5.3 Depth-area-duration curves

Areal rainfall amounts are crucial drivers of the hydrologic response and are important for understanding rainfall structure and triggering mechanisms (e.g., Armon et al., 2018; Durrans et al., 2002; Kalma and Franks, 2003; Zepeda-Arce et al., 2000). To quantify and compare observed and simulated areal rainfall amounts, we used depth-area-duration (DAD) curves, which represent the areal extent in which given rainfall depths over given durations are exceeded (Zepeda-Arce et al., 2000).

3.5.4 Autocorrelation structure of rain fields

High-intensity, small-scale convective rain cells are among the main factors generating flash-floods in small, mountainous and desert catchments (e.g., Armon et al., 2018; Doswell et al., 1996; Merz and Blöschl, 2003), and their fine spatiotemporal structure directly affects the potential of rain-gauge monitoring (Marra and Morin, 2018). To analyse the convective rain structure we computed, from both the observed radar-QPE and from the WRF output, the spatial autocorrelation structure of the maps containing convective elements using the methodology presented by Marra and Morin (2018). We interpolated the radar-QPE to 10-min time intervals to match the model temporal resolution, and defined as convective rainfall fields all the



rain maps in which at least one convective rain cell, defined as a connected region $\geq 3 \text{ km}^2$ with rain intensity exceeding 10 mm h^{-1} and including at least one pixel exceeding 25 mm h^{-1} , is observed (Marra and Morin, 2018). We computed the 2-D spatial autocorrelation function of the convective fields following the method in Nerini et al. (2017). A three-parameter exponential function (Eq. 1) was fitted to the 2-D spatial autocorrelation to quantify the correlation distance:

$$r(h) = ae^{-\left(\frac{h}{b}\right)^c}, \quad (1)$$

where h is the lag distance, b is the correlation distance (the distance in which correlation drops to $r = e^{-1}$), and a and c are the nugget and shape parameters of the curve, respectively. Eq. 1 results in an approximation of the 1-D autocorrelation function of convective rain fields. Spatial heterogeneity of the of the autocorrelation field is quantified calculating the deviation of the 2-D autocorrelation field from isotropy, following the approach in Marra and Morin (2018). To that end, we defined the ellipticity of the 2-D autocorrelation as the ratio of the minor to major axis of the (approximated) ellipse encompassing the $r = e^{-1}$ region of the spatial autocorrelation field.

The temporal autocorrelation is computed converting the 2-D spatial domain to a 1-D array and adopting time as the second dimension, as proposed by Marra and Morin (2018). It is worth noting that the computed temporal correlation distance neglects advection (Eulerian perspective), and is therefore shorter than the correlation distance one would obtain in a Lagrangian perspective.

4. Results

4.1 Model skill

4.1.1 Bias

Figure 3 shows the rainfall accumulated throughout all HPEs as estimated by the weather radar, modelled by the WRF, and measured by rain gauges (Fig. 3a, b and d, respectively). The bias, defined here as the ratio between WRF-rainfall and radar QPE, is shown in Fig. 3c. In 69% of the studied region, the bias lies between 3 and 1/3 while some areas show a strong positive bias (Fig. 3c). The three stations highlighted in the figure (the values shown for radar and WRF represent the average of the 9 pixels surrounding the gauge locations) show how this large bias is mostly caused by radar underestimation. In fact, these areas are generally located far from the radar or in the eastern portion of the radar coverage, where radar QPE suffers from range degradation and beam overshooting due to the presence of mountains. In other areas, the bias seems related to residual beam blockages. Bias smaller than 1 is also apparent in regions with ground clutters, and some spatial inconsistencies related to the interpolation of a few fully blocked beams can also be noticed. To avoid this radar estimation inaccuracies interfering with our results, hereinafter we focus only on the areas in which the bias lies between 3 and 1/3 (Fig. 3c).



250 4.1.2 Visual, neighbourhood and object-based evaluation of WRF model forecasts

Visual comparison of observed (radar) and simulated (WRF) rainfall fields yielded mostly (subjectively) good results in terms of the spatial rainfall patterns, such as widespread vs. localised rainfall (e.g., Fig. 4a-c, in which the first HPE in the list in Table S1 is shown). The spatial frequency is also generally well represented (Fig. 4d). At the same time, pixel-based comparisons are deemed inappropriate for such an analysis, as shown in the scatter plot (Fig. 4e). These observations are true
255 for most of the examined HPEs, with the exception of two HPEs in which the WRF model clearly failed in representing the rainfall patterns (e.g., one example in Fig. 5). Both these poorly simulated HPEs were characterised by relatively short total storm durations (1.7 and 2 days) just exceeding the durations that defined them as HPEs (6 h and 3-24 h, respectively). Synoptically they are classified as ARSTs, a system generally characterised by local, short living convection associated with localised rainfall triggering mechanism (Armon et al., 2018). Mesoscale models (e.g., WRF) skill is poorer in simulating this
260 type of events, mainly due to their short predictability and stochastic nature (see e.g., Yano et al., 2018). Although a deeper understanding of these aspects can be beneficial for improving future simulations, it falls beyond the scope of this study and will need future dedicated research efforts.

The FSS of the first HPE (Fig. 4f) further manifests the accuracy of the simulated rainfall fields. The forecast has a larger FSS than the uniform FSS for all cumulative rainfall ≤ 50 mm, even at the model resolution (1 km). For larger cumulative rainfall
265 (but < 125 mm), the FSS is still higher than the uniform FSS, when spatially averaged (e.g., 40 km averaging for cumulative rain of 100 mm). Only for the higher rainfall amounts, e.g., 125 mm, greater than 99% of pixels in this HPE, the model forecast is unskilled, i.e., the uniform FSS outperforms the WRF forecast FSS.

During EM rainstorms, cumulative rainfall values are distributed unevenly in space, and extremely high rainfall depths are embedded within the larger aerial coverage of lower rainfall depths (e.g., Armon et al., 2018; Dayan and Morin, 2006; Morin
270 et al., 2007). Forecasting the spatial distribution (location and spatial frequency) of low cumulative rainfall is thus easier than forecasting the distribution of the high end of cumulative rainfall, even when averaging is conducted over large scales. The minimal scale (Roberts and Lean, 2008) at which the FSS of the model's forecast is higher than the uniform FSS was calculated for cumulative rainfall of 1-200 mm, for all of the identified HPEs (Fig. 6). This allows estimating the minimal scales for skilful forecasts for various cumulative rain depths. For example, the original model resolution yields a skilful forecast for
275 cumulative rainfall depths of < 25 mm in 50% of the HPEs (Fig. 6). The figure also shows that cumulative rainfall exceeding 45 mm, in most of the cases, are skilfully forecasted only at relatively large spatial scale (tens of kilometres).

The SAL analysis (Fig. 7) shows a good performance of the model, except for a substantial positive amplitude bias (inter-event amplitude component median = 0.80 [i.e. bias of 2.3, as defined above], interquartile range = 0.37-1.02). Two events stand out with a bias smaller than one; these are the abovementioned poorly simulated HPEs. The structure component is well
280 modelled in most cases, showing the ability of the WRF to accurately generate precipitation objects (0.06 and -0.06 to +0.26, median and interquartile range, respectively). This is particularly important in regions and events where rainfall is generated



through both convective and stratiform processes, or when intense rainfall is embedded within a larger-scale low intensity precipitation (Wernli et al., 2009).

Relatively low values of the location component (0.25 and 0.18-0.31, median and interquartile range, respectively) demonstrate the high capability of the model to spatially distribute precipitation objects. Medially, 34% of this component is composed of the error in the centre of mass location (i.e., a median error of 30 km in the location of the centre of mass), and the rest is from the average location of each precipitation object. Namely, the model prediction of the centre of mass of the rain field is quite satisfying, but the prediction of individual precipitation objects is poorer. Standing out with high location values (0.46 and 0.85) are the same two challenging HPEs, in which the model was unable to simulate the rainfall in a satisfying manner, yielding biases smaller than one and large spatial inconsistency with respect to observations (see above, e.g., Fig. 5).

The overall positive bias, seen in the amplitude component (Fig. 7), could result both from underestimation of the radar QPE or overestimation of the WRF simulations. Possible reasons leading to radar underestimation were discussed above, and may contribute to this bias even after the most severely biased regions have been masked. However, this positive bias still needs to be taken into account when addressing the actual cumulative rainfall amounts predicted by the model.

The overall good representation of precipitation objects implies that precipitation processes generated by the model represent actual processes and rainfall characteristics (Wernli et al., 2009).

4.2 Characterisation of rainfall patterns

4.2.1 General properties of HPEs

According to the definition applied in this study, a given event can be considered as HPE for more than one duration. This could happen when the thresholds associated with the selected durations (Sect. 3.3) are exceeded either at the same location or when they are exceeded in different regions. The durations associated with each HPE are listed in Table S1. The co-occurrence of each HPE-duration with the rest of the examined durations is shown on Fig. 8; these co-occurrence values are similar to values determined in the Alps by Panziera et al. (2018). For example, 79% of the HPEs at 24 h duration are also HPEs at 72 h duration. Fig. 8 indicates that there is a high dependency (i.e. co-occurrence) of the short-duration HPEs (3-12 h). Similarly, there is a high dependence within the long duration (24-72 h) HPEs. Nevertheless, even the shortest duration HPEs examined here, show a rather high co-occurrence with longest duration HPEs (probabilities in all cases ≥ 0.5).

Despite the identification of HPEs depended on quality and availability of radar data and only 41 HPEs were available after quality check, this analysis can be considered as “semi-climatological”, as the selected HPEs do not exhibit obvious biases with respect to the climatology of HPEs: (a) the seasonality is following the seasonal pattern of EM rainy days (Fig. 9), although HPEs occur more frequently during the beginning of the winter, presumably due to the high sea surface temperatures; (b) HPEs are identified throughout the radar archive (with zero to seven HPEs per year); (c) the frequency of the prevailing synoptic circulation patterns during HPEs (Table S1) resembles the frequency observed during rainy days (Marra et al., 2019); and (d) HPEs characterised by ARST prevalence are common only during the transition seasons (Fig. 9) (e.g., De Vries et al., 2013).



For most durations, rain amounts defining the HPEs are larger near the Mediterranean coast, extending a few kilometres off-
315 and on-shore (Fig. 2). This resembles the observed pattern of high rain intensities near the coast, rather than inland (Karklinsky
and Morin, 2006; Peleg and Morin, 2012; Sharon and Kutiel, 1986), also reported for extreme precipitation quantiles observed
from both weather radar and satellite sensors (Marra et al., 2017). In contrast, short durations (<12 h) exhibit the highest rain
intensities in the arid portions of the region. The frequency of rain in the arid areas is lower than in the rest of the region
(Goldreich, 2012); thus, the 99.5% quantiles are based on fewer data. Yet, the reported higher extreme rain amounts for shorter
320 durations are in agreement with previous studies, which showed that highly localised convective rainfall is more common
during HPEs in the desert than in other climate environments in the EM (Marra et al., 2017; Marra and Morin, 2015; Sharon,
1972). In the mountains, the case is the opposite; rainfall is produced more significantly through stratiform (or shallow
convection) processes, and, therefore, rain amounts for short durations are relatively lower (Sharon and Kutiel, 1986). For the
longer durations, rain intensities in the mountains are comparable to the intensities near the coast, resulting probably from the
325 tendency of rain to persist in orography affected regions (e.g., Panziera et al., 2015; Tarolli et al., 2012).

Affected by higher rain intensities, the centre of mass of the precipitation field for all HPEs is located near the EM coastline
(Fig. 10). Nevertheless, a seasonal pattern appears, with a general landward shift of the centre of mass during the rainy season
(Fig. 10). This is caused by land-sea differential heating and heat capacities, and resembles the seasonal pattern of rain
intensities in the EM (Goldreich, 1994; Sharon and Kutiel, 1986). In fact, this points out the observed preference of convective
330 clouds to form above high-temperature surfaces, i.e., the sea surface or nearby coastal plains in autumn or early winter, and
farther inland in spring. The exact location of the centre of mass depends on the ability of the radar to produce accurate QPE
over the region. Due to the range degradation typical to radar rainfall estimates, the centre of mass is biased towards the radar
location. This is confirmed also by the WRF results, showing a more widespread distribution of the centres of mass. In terms
of seasonality, the simulated centres of mass exhibit a similar, even if slightly less obvious, landward pattern.

335 4.2.2 Areal rainfall

We show in Fig. 11 the depth-are-duration (DAD) curves obtained from all the 41 HPEs for durations of 30 min, 6 h and 24 h
from radar QPE (Fig. 11a, c, and e, respectively) and WRF (Fig. 11b, d, and f). A major increase in cumulative rainfall with
increased durations is observed both for the radar and for the WRF curves (Fig. 11g): e.g., based on the radar, an area of 10^3
340 km^2 is medially covered by 9 mm for a duration of 0.5 h, which increases to 35 mm and 60 mm for 6 and 24 h, respectively
(corresponding values from the WRF-derived rainfall are 4, 25 and 50 mm). This increase could be explained either by
continuous rainfall, or by frequent arrival of rain cells into the region. The latter increases the wet area and the cumulative
rainfall in areas that already experienced rainfall, and is a major characteristic of HPEs in the EM (e.g., Armon et al., 2018,
2019; Sharon, 1972). Furthermore, over the longer durations, this causes DAD curves for different events to be more similar
one another (e.g., Fig. 11e, and f).

345 The inter-event spread and the difference in the DAD curves for MC and ARST (Fig. 11a-f), illustrate the various types of
HPEs identified here. These types range between rainstorms exhibiting only a minimal increase in rainfall area through time,



i.e. almost all rainfall precipitates during a short period, and rainstorms composed of many rain cells passing through the same area, or long-lasting rainstorms. These results confirm previous findings by Armon et al. (2018), based on a more limited number of events: HPEs classified as ARSTs (Table S1) tend to be of higher rain intensities for smaller regions and shorter periods than HPEs classified as MCs. MCs only exhibit higher rain intensities over larger regions and for longer durations. It is important to note the difference between radar-QPE and WRF-derived rainfall DAD curves. Higher rain values in the radar-QPE over the range of smaller areas is the most obvious difference (Fig. 11g). Although these higher values may, at a first sight, point out that the WRF is unable to reproduce the high-intensity rainfall of the HPEs in the EM, it should be reminded that at short durations high intensity radar QPEs can be of lower accuracy due to contamination from residual ground clutter or hail. This may affect more selectively the QPEs of the smaller areas. For instance, for one of the HPEs, an area >100 km² has rain amount ≥ 100 mm in 0.5 h (Fig. 11a), a value that exceeds 200-yr return period for the area (Morin et al., 2009). Other notable differences are some ARST-classified HPEs with WRF-derived DAD curves (Fig. 11b, d, and f), consisting of the two WRF-unresolved HPEs mentioned above, and yielding a median ARST curve that is much lower than the radar-derived curve.

The reported differences between WRF- and radar-derived curves result in an overall greater area-over-threshold radar curves for the high rainfall thresholds, especially for the short durations. For long durations and low rainfall thresholds, the WRF area is larger (Fig. 11), reflecting the positive bias probably related to radar range degradation and beam overshooting.

4.2.3 Autocorrelation structure of convective rainfall

HPEs in the EM are commonly composed of highly localised convective rain cells. This is well shown by the sharp decrease of the 1-D autocorrelation describing the convective rain fields (Fig. 12a and b) obtained using all the convective rain fields throughout the 41 HPEs (n=11731 snapshots for radar and n=14323 for WRF). The median decorrelation distance (defined as the distance in which correlation drops to $r = e^{-1}$, i.e., the parameter b of the 1-D exponential fit [Eq. 1]) of all convective rain snapshots from the radar data is ~9 km (~7 km using the WRF derived rainfall) and ranges between 3 and 23 km (for the 10% and 90% quantiles; 2 and 20 km using WRF). These values are comparable with previously reported observations (e.g., Ciach and Krajewski, 2006; Morin et al., 2003; Peleg and Morin, 2012; Villarini et al., 2008) and are somewhat larger than the reported values for the south-eastern part of the area by Marra and Morin (2018). However, it must be noted that Marra and Morin (2018) examined 1-min rainfall fields versus the 10-min fields examined here.

The median of the temporal decorrelation distance (Fig. 12c and d) is ~4 min (~14 min for the WRF) and it ranges between <1 and 19 min (10% and 90% quantiles; 3 and 29 min using WRF). Despite agreeing with the results of Marra and Morin (2018), the exact temporal decorrelation distance is somewhat dubious, since it is shorter than the time-step used for its calculation (10 min). The larger temporal correlation in the WRF-derived rainfall is expected, because radar QPE suffers from temporal inconsistencies (e.g., when a convective cell passes through a region with beam blockages). Nevertheless, such short temporal decorrelation confirms the local and spotty nature of rainfall characterising HPEs in the region.



The declining pattern of the 1-D autocorrelation overlooks the 2-D spatial heterogeneity of the autocorrelation field. The ellipticity of the 2-D autocorrelation yielded a median value of 0.56 (0.58 for the WRF), with a range of 0.33-0.80 (10%-90% quantiles; 0.33-0.79 using WRF). These autocorrelation ellipses in the radar data were oriented 13° anti-clockwise from the E-W axis (median value) and 25° for the WRF ellipses, similarly to the orientation of radar rain cells orientation in the eastern part of the region (Belachsen et al., 2017), but somewhat different from the orientation of the autocorrelation fields from the south-eastern part of the region (Marra and Morin, 2018). This orientation represents the general alignment of rain cells during a HPE, accounting for cells during the beginning of the event (which probably tend to the SW direction) and during its end (shifting towards NW). Therefore, they are oriented more anti-clockwise than the autocorrelation fields from the south-eastern part of the region (Marra and Morin, 2018), which commonly represents rainfall during the end of a rainstorm (Armon et al., 2019). Moreover, Marra and Morin (2018) examined 1-min snapshots while here advection can play a role in the examined 10-min time interval. Finally, Marra and Morin (2018) analysed only 11 events, thus, inter-event variance may still play a large role in their results. The high agreement between modelled and observed rain field ellipticity and orientation also demonstrate the high skill of the WRF simulations to accurately represent convection in the region and, thus, reproduce rain-cell properties.

5. Discussion and summary

This work characterises rainfall patterns during 41 HPEs in the EM and evaluates the ability of a high-resolution WRF model to properly simulate their cumulative rain field, and their spatiotemporal behaviour, with a specific emphasis to their convective component. If this effort is successful it will open the way to downscaling of global climate projections into induced changes in rainfall patterns at a regional scale during HPEs, including the understanding of the strengths and weaknesses of the regional results.

To overcome the diverse climatology of the EM, we identified HPEs using a pixel-based weather radar climatology. We used a uniquely long, quality-controlled and gauge-adjusted, high-resolution weather radar archive to characterise the rainfall patterns. A convection-permitting high-resolution WRF model configuration was used to simulate the same HPEs and the results of this modelling effort were compared to the radar QPE. For most of the 41 HPEs, model simulations resulted in valuable results: using the Fractions Skill Score we determine that (a) WRF simulations are highly accurate for cumulative rainfall <25 mm (Fig. 6; Sect. 4.1.2), (b) accumulations of >45 mm produce variable results among different cases (Figs. 4, 5 and 6 Sect. 4.1.2). I.e., skilful results are gained if the model output is averaged over at least a few tens of kilometres. Structure-Amplitude-Location analysis of cumulative rainfall shows that rainfall location and structure are correctly reproduced by the model and is similar to the observed by the weather radar data in 39 out of the 41 HPEs. Conversely, rainfall amplitude is highly (positively-) biased, with some of the bias likely explained by radar underestimation; however, a model positive bias cannot be excluded.



410 In general, rain amounts forming HPEs are higher near the EM coastline with the exceptions of (a) short durations, for which
the highest rain amounts are observed in the desert regions, and (b) the longer-duration HPEs, for which mountainous rain
amounts are comparable to the ones at the coast. Identified HPEs occur during the wet season (October-April), and, primarily,
in November-February. Their centre-of-mass is close to the Mediterranean coastline and shifts landward during the season.
We analysed the areal distribution of rainfall at various durations, the autocorrelation structure of the convective rainfall fields
415 and depth-area-duration curves, obtaining quantitative information on the characteristics of the rainfall fields, on the ability of
WRF to simulate them, and on the processed generating them, such as the aggregation of small and short living rain cells to
produce a HPE.

5.1 Spatial distribution of rain intensity thresholds defining HPEs

High intensity thresholds forming HPEs near the Mediterranean Sea (Fig. 2) are expected, because of its warm surface waters
420 and high moisture fluxes, and are also apparent in other regions of the Mediterranean (e.g., Dayan et al., 2015; Ivatek-Šahdan
et al., 2018; Khodayar et al., 2018; Pastor et al., 2002; Peleg et al., 2018; Tarolli et al., 2012). High rain intensities in the desert
are somewhat more intriguing. For example, Warner (2004) mentioned that there are hither and tither observations of whether
rain intensities in the desert are higher than in non-desert regions. An opposing trend between mean annual rainfall and short-
duration rain intensities was also described by Sharon and Kutiel (1986) using rain gauges and by Marra and Morin (2015)
425 using both rain gauges and weather radar. This trend is related to higher surface temperatures in desert regions, that may
enhance convective activity (e.g., Peleg et al., 2018), associated to a deeper boundary layer (e.g., Gamo, 1996; Marsham et al.,
2013) and to the prevailing of rainfall from ARSTs circulation patterns, which generally cause higher rain intensities (Armon
et al., 2018; Nicholson, 2011; Sharon and Kutiel, 1986; De Vries et al., 2013). Such a sharp spatial change in the climatology
of the rain intensities defining HPEs may only be captured using high-resolution, high spatiotemporal coverage data (such as
430 the radar-QPE presented here), and reproduced by high-resolution, convection-permitting models.

5.2 Multiple duration HPEs and their relation to flash floods

Mediterranean and, even more, desert climate HPEs, can produce rain amounts of the same order of magnitude of the mean
annual rainfall (e.g., Nicholson, 2011; Schick, 1988; Tarolli et al., 2012). Frequent co-occurrence of short and long duration
HPEs is thus to be expected, and dividing events into short versus long duration HPEs is not straightforward. However, our
435 dataset comprises events of different characteristics: local and intense, as well as widespread; rainfall triggering mechanisms
and potential hydrologic impact can be quite different.

Zoccatelli et al. (2019) observed a relatively high correlation between rain depths over a catchments and unit peak discharge
in catchment areas ranging between 13-1232 km² of Mediterranean and desert environments in the EM. In arid and semi-arid
catchments, high correlation was reported between the storm rain core, defined as the largest hourly intensity over a 9 km²
440 area in the catchment, and the unit peak discharge. Floods in Mediterranean catchments were accompanied by larger rain
depths (~52 mm) over longer durations (~1 day), compared to the desert catchments (~14 mm, ~7 h). Comparison of these



values with the DAD curves in Fig. 11, show that a portion of the here analysed HPEs are prone to produce floods in smaller catchments and in the desert regions, while others could generate floods in larger catchments and in the Mediterranean climate region. Specifically, the convective part of the rainstorm is known to generate the highest-magnitude floods, even at the
445 Mediterranean climate areas (e.g., Rinat et al., 2018; Tarolli et al., 2012). The short spatiotemporal autocorrelation distances observed for the convective rain fields highlight once again the spottiness of rainfall of HPEs in the EM region (Sharon, 1972) and was well-simulated by the WRF model (Fig. 12).

5.3 Identification and characterisation of HPEs using weather radar and high-resolution weather model

ARST synoptic circulation is often associated to flash floods in the desert part of the region (Ashbel, 1938; Kahana et al., 2002;
450 Krichak et al., 1997) and its rainfall is commonly caused by mesoscale triggering of convection (Armon et al., 2018) and is therefore less predictable (e.g., Keil et al., 2014). It is thus crucial for future studies to understand the reasons for poor modelling results observed in two (of 41) of these HPEs. Possible aspects to be inspected include the adopted parametrisation schemes (Table 1) but, since we used a convection-permitting resolution, problems could arise from other issues. In particular, since errors in the moisture field tend to propagate fast, the correct amount of moisture should be entered to the model in the
455 correct location to properly reproduce rainfall at the mesoscale (e.g., Rostkier-Edelstein et al., 2014; Zhang et al., 2007). In this study we used ERA-Interim reanalysis data (~80 km horizontal resolution), which may not be accurate enough to resolve some conditions, but is at the same scale as outputs of global climate model. Future studies should consider using higher resolution input data, such as the newly released ERA5 data (Hersbach, 2016).

The use of a long record of radar QPE enabled us high-resolution semi-climatological characterisation of the rainfall patterns
460 during HPEs with a resolution and spatial coverage that cannot be achieved using rain gauges. However, rainfall characteristics could not be adequately retrieved in regions suffering from radar data acquisition problems. Despite this, the resulted skill of the WRF rainfall fields support its use for representing HPEs in regions not well covered by radars. Since the analyses were performed in a region exhibiting a strong climatic gradient, we suggest that similar results should be obtained in other parts of the world, at least in areas characterised by similar climates.

465 Nonetheless, the use of a deterministic convection-permitting model is still unsatisfactory in pinpointing the highest observed rain accumulations. Although such models are becoming more common in weather and climate forecasting and research (Prein et al., 2015), they are still not adequate for short-term hydrological applications, such as flash-flood predictions. The structure of high cumulative rain is predicted quite well. However, it still suffers from a positive bias, and is not exactly well located (e.g., Figs. 6 and 7). In order to provide better flood predictions, especially for small catchments and for flash flood generation
470 controlled by infiltration-excess, there is a need for more structured approaches, such as ensemble forecasts and data assimilation of meteorological observations (e.g., Diomede et al., 2014; Gustafsson et al., 2018; Hamill et al., 2008; Rostkier-Edelstein et al., 2014). These would provide probabilistic (rather than deterministic) information, and could therefore account for the uncertainty characterising the location in high-resolution models (e.g., Alfieri et al., 2012; Vincendon et al., 2011).



475 Characterisation of rainfall patterns during HPEs has a special significance in the EM: on the one hand, the region suffers from
a severe water shortage and, on the other hand, is prone to devastating floods. Both are predicted to worsen in response to
climate change (e.g., Alpert et al., 2002; Kelley et al., 2015; Sowers et al., 2010). Modelling could help understanding the
effects of climate change on these two aspects but, before assessing the projections for a change in rainfall patterns induced
by climate change, we need to consider what aspects of these patterns are still not well captured by weather models at present.
These aspects will thus be a challenge in future predictions. For example, we showed here that rainfall during ARSTs is less
480 adequately forecasted. These ARST HPEs are notably known to cause flash floods, and, as ARSTs might be occurring more
frequently due to global warming (Hochman et al., 2018b), this low predictability should be addressed.

The work presented above is a step towards better understanding of rainfall patterns during HPEs in the EM, and we are
currently extending the research to relate specific rainfall patterns and atmospheric conditions at a high-resolution, and to
analyse how the predicted climate change will affect the same rainfall characteristics we outlined above. An additional research
485 direction worth following is to combine our procedures with satellite-based climatology. However, to date, satellite products
present insufficient temporal (≥ 0.5 h, mostly ≥ 3 h) and spatial ($\geq 0.04^\circ$, mostly $\geq 0.25^\circ$) resolutions (e.g., Ashouri et al., 2015;
Gehne et al., 2016) to adequately sample the fine scale properties of convective rainfall fields, particularly in arid areas.

6. Conclusions

This study presents the identification of HPEs using a weather radar. These HPEs were then simulated using a high-resolution
490 weather model and evaluated, focusing on the spatiotemporal patterns of the rainfall fields. The main conclusions of this
characterisation and evaluation are summarised below:

- HPEs in the EM are common between October and April, and their occurrences are focused in November-February. HPEs centre of mass is located near the Mediterranean coastline and moves landward during the rainy season.
- For most storm durations, the rain amounts forming HPEs (i.e., larger than 99.5% of all rainy hours) are higher near
495 the Mediterranean coast. For short durations, the highest HPE rain amounts are located in the desert, and for long
durations mountainous and coastal regions exhibit similar values.
- HPEs consist of small convective rain cells (spatial and temporal decorrelation of ~ 9 km and ~ 4 min, respectively)
that form a highly variable rainy area over short durations. The size of the rainy region increases with duration and
becomes more homogenous between events.
- Convection-permitting high-resolution WRF model can simulate most HPEs, apart from some of the shortest, most
500 localised storms.
- Rainfall structure is well simulated. Nevertheless, it is slightly less variable than the observed one, and is
characterised by a significant positive bias in the rain volume. This can be, at least partially, attributed to radar
underestimations.



- 505
- The location of rainfall is generally predicted properly, with the exception of the highest rainfall amounts: the minimal scale for forecasting total rainfall depths >25 mm is highly variable between events, and increases significantly for rainfall depths >45 mm.

Using high-resolution weather model that can reproduce rainfall patterns in times of HPEs is of great importance in predicting hydrometeorology of flood-producing rainstorms. However, these must be elaborated, using e.g. ensemble runs of the model.

- 510
- Convection-permitting models may also help in assessing changes in precipitation induced by climate change, although if those are composed of HPEs that are less-skilfully predicted in present, they should be examined cautiously.

7. Author contribution

MA and EM conceptualise this work. Data curation and formal analysis were performed by MA and FM. Funding acquisition was made by EM, YE, FM and DRE. Supervision by EM and YE. MA wrote the original draft of this paper, which was reviewed and edited by all authors.

515

8. Data availability

Rain gauge data were provided and pre-processed by the Israel Meteorological Service (www.ims.gov.il). Shacham radar data were provided by EMS-Mekorot projects (www.emsmekorotprojects.com). ERA-Interim data were downloaded from the Research Data Archive at the National Center for Atmospheric Research, Computational and Information Systems Laboratory: European Centre for Medium-Range Weather Forecasts, 2012, updated monthly. ERA-Interim Project, Single Parameter 6-Hourly Surface Analysis and Surface Forecast Time Series: <https://doi.org/10.5065/D64747WN>. WRF namelist files are available upon request from the corresponding author.

520

9. Competing interests

The authors declare that they have no conflict of interest.

525 10. Acknowledgments

This study is a contribution to the PALEX project “Paleohydrology and Extreme Floods from the Dead Sea ICDP Core”, funded by the DFG (Grant BR2208/13-1/-2). It is also partially funded by the Israel Science Foundation (1069/18), the NSF–BSF (BSF 2016953), the Israel Ministry of Science and Technology (grant no. 61792), the Advanced School for Environmental Studies at the Hebrew University of Jerusalem, and the Israel Water Authority, and is a contribution to the HyMeX program.

530

The authors thank Prof. Pinhas Alpert for the updated synoptic classification data.



References

- Ahlborn, M., Armon, M., Ben Dor, Y., Neugebauer, I., Schwab, M. J., Tjallingii, R., Shoqeir, J. H., Morin, E., Enzel, Y. and Brauer, A.: Increased frequency of torrential rainstorms during a regional late Holocene eastern Mediterranean drought, *Quat. Res.*, 89(2), 425–431, doi:10.1017/qua.2018.9, 2018.
- 535 Alfieri, L., Thielen, J. and Pappenberger, F.: Ensemble hydro-meteorological simulation for flash flood early detection in southern Switzerland, *J. Hydrol.*, 424–425, 143–153, doi:10.1016/j.jhydrol.2011.12.038, 2012.
- Alpert, P. and Shay-EL, Y.: The moisture Source for the Winter Cyclones in the Eastern Mediterranean, *Isr. Meteorol. Res. Pap.*, 5, 20–27, 1994.
- Alpert, P., Ben-Gai, T., Baharad, A., Benjamini, Y., Yekutieli, D., Colacino, M., Diodato, L., Ramis, C., Homar, V., Romero, R., Michaelides, S. and Manes, A.: The paradoxical increase of Mediterranean extreme daily rainfall in spite of decrease in total values, *Geophys. Res. Lett.*, 29(11), 1536, doi:10.1029/2001GL013554, 2002.
- 540 Alpert, P., Osetinsky, I., Ziv, B. and Shafir, H.: Semi-objective classification for daily synoptic systems: Application to the eastern Mediterranean climate change, *Int. J. Climatol.*, 24(8), 1001–1011, doi:10.1002/joc.1036, 2004.
- Amponsah, W., Ayral, P. A., Boudevillain, B., Bouvier, C., Braud, I., Brunet, P., Delrieu, G., Didon-Lescot, J. F., Gaume, E., Lebouc, L., Marchi, L., Marra, F., Morin, E., Nord, G., Payrastré, O., Zoccatelli, D. and M., B.: Integrated high-resolution dataset of high intensity Euro-Mediterranean flash floods, *Accept. Publ. Earth Syst. Sci. Data*, 2018.
- 545 Anthes, R. A., Kuo, Y.-H., Baumhefner, D. P., Errico, R. M. and Bettge, T. W.: Predictability of Mesoscale Atmospheric Motions, *Adv. Geophys.*, 28, 159–202, doi:10.1016/S0065-2687(08)60188-0, 1985.
- Armon, M., Dente, E., Smith, J. A., Enzel, Y. and Morin, E.: Synoptic-scale control over modern rainfall and flood patterns in the Levant drylands with implications for past climates, *J. Hydrometeorol.*, 19(6), 1077–1096, doi:10.1175/JHM-D-18-0013.1, 2018.
- 550 Armon, M., Morin, E. and Enzel, Y.: Overview of modern atmospheric patterns controlling rainfall and floods into the Dead Sea: Implications for the lake's sedimentology and paleohydrology, *Quat. Sci. Rev.*, 216, 58–73, doi:10.1016/j.quascirev.2019.06.005, 2019.
- 555 Ashbel, D.: Great floods in Sinai Peninsula, Palestine, Syria and the Syrian Desert, and the influence of the Red Sea on their formation, *Q. J. R. Meteorol. Soc.*, 64(277), 635–639, 1938.
- Ashouri, H., Hsu, K. L., Sorooshian, S., Braithwaite, D. K., Knapp, K. R., Cecil, L. D., Nelson, B. R. and Prat, O. P.: PERSIANN-CDR: Daily precipitation climate data record from multisatellite observations for hydrological and climate studies, *Bull. Am. Meteorol. Soc.*, 96(1), 69–83, doi:10.1175/BAMS-D-13-00068.1, 2015.
- 560 Ban, N., Schmidli, J. and Schär, C.: Evaluation of the convection-resolving regional climate modeling approach in decade-long simulations, *J. Geophys. Res.*, 119(13), 7889–7907, doi:10.1002/2014JD021478, 2014.
- Belachsen, I., Marra, F., Peleg, N. and Morin, E.: Convective rainfall in a dry climate: Relations with synoptic systems and flash-flood generation in the Dead Sea region, *Hydrol. Earth Syst. Sci.*, 21(10), 5165–5180, doi:10.5194/hess-21-5165-2017,



- 2017.
- 565 Bližňák, V., Kašpar, M. and Müller, M.: Radar-based summer precipitation climatology of the Czech Republic, *Int. J. Climatol.*, 38(2), 677–691, doi:10.1002/joc.5202, 2018.
- Bloschl, G. and Sivapalan, M.: Scale Issues in Hydrological Modelling: a Review, *Hydrol. Process.*, 9, 251–2901 [online] Available from: papers2://publication/uuid/EB5C42FF-17C4-4FF1-8216-E985A0ED7C96, 1995.
- Bogaard, T. A. and Greco, R.: Landslide hydrology: from hydrology to pore pressure, *Wiley Interdiscip. Rev. Water*, 3(3),
570 439–459, doi:10.1002/wat2.1126, 2016.
- Borga, M. and Morin, E.: Characteristics of Flash Flood Regimes in the Mediterranean Region, in *Storminess and Environmental Change Climate Forcing and Responses in the Mediterranean Region*, edited by N. Diodato and G. Bellocchi, pp. 65–76, Springer Netherlands, Dordrecht., 2014.
- Borga, M., Boscolo, P., Zanon, F. and Sangati, M.: Hydrometeorological Analysis of the 29 August 2003 Flash Flood in the
575 Eastern Italian Alps, *J. Hydrometeorol.*, 8(5), 1049–1067, doi:10.1175/JHM593.1, 2007.
- Borga, M., Anagnostou, E. N., Blöschl, G. and Creutin, J. D.: Flash flood forecasting, warning and risk management: The HYDRATE project, *Environ. Sci. Policy*, 14(7), 834–844, doi:10.1016/j.envsci.2011.05.017, 2011.
- Borga, M., Stoffel, M., Marchi, L., Marra, F. and Jakob, M.: Hydrogeomorphic response to extreme rainfall in headwater systems: Flash floods and debris flows, *J. Hydrol.*, 518(PB), 194–205, doi:10.1016/j.jhydrol.2014.05.022, 2014.
- 580 Cassola, F., Ferrari, F. and Mazzino, A.: Numerical simulations of Mediterranean heavy precipitation events with the WRF model: A verification exercise using different approaches, *Atmos. Res.*, 164–165, 210–225, doi:10.1016/j.atmosres.2015.05.010, 2015.
- Ciach, G. J. and Krajewski, W. F.: Analysis and modeling of spatial correlation structure in small-scale rainfall in Central Oklahoma, *Adv. Water Resour.*, 29(10), 1450–1463, doi:10.1016/j.advwatres.2005.11.003, 2006.
- 585 Collier, C. G.: Flash flood forecasting: What are the limits of predictability?, *Q. J. R. Meteorol. Soc.*, 133(622), 3–23, doi:10.1002/qj.29, 2007.
- Cristiano, E., ten Veldhuis, M.-C. and van de Giesen, N.: Spatial and temporal variability of rainfall and their effects on hydrological response in urban areas -- a review, *Hydrol. Earth Syst. Sci.*, 21(7), 3859–3878, doi:10.5194/hess-21-3859-2017, 2017.
- 590 Davis, C., Brown, B. and Bullock, R.: Object-Based Verification of Precipitation Forecasts. Part I: Methodology and Application to Mesoscale Rain Areas, *Mon. Weather Rev.*, 134(7), 1772–1784, doi:10.1175/MWR3145.1, 2006.
- Dayan, U. and Morin, E.: Flash flood – producing rainstorms over the Dead Sea: A review, *New Front. Dead Sea Paleoenviron. Res. Geol. Soc. Am. Spec. Pap.*, 401(04), 53–62, doi:10.1130/2006.2401(04)., 2006.
- Dayan, U., Ziv, B., Margalit, A., Morin, E. and Sharon, D.: A severe autumn storm over the Middle-East: Synoptic and
595 mesoscale convection analysis, *Theor. Appl. Climatol.*, 69(1–2), 103–122, doi:10.1007/s007040170038, 2001.
- Dayan, U., Nissen, K. and Ulbrich, U.: Review Article: Atmospheric conditions inducing extreme precipitation over the eastern and western Mediterranean, *Nat. Hazards Earth Syst. Sci.*, 15(11), 2525–2544, doi:10.5194/nhess-15-2525-2015, 2015.



- Dee, D. P., Uppala, S. M., Simmons, A. J., Berrisford, P., Poli, P., Kobayashi, S., Andrae, U., Balmaseda, M. A., Balsamo, G., Bauer, P., Bechtold, P., Beljaars, A. C. M., van de Berg, L., Bidlot, J., Bormann, N., Delsol, C., Dragani, R., Fuentes, M.,
600 Geer, A. J., Haimberger, L., Healy, S. B., Hersbach, H., Hólm, E. V., Isaksen, L., Kållberg, P., Köhler, M., Matricardi, M., McNally, A. P., Monge-Sanz, B. M., Morcrette, J.-J., Park, B.-K., Peubey, C., de Rosnay, P., Tavolato, C., Thépaut, J.-N. and Vitart, F.: The ERA-Interim reanalysis: configuration and performance of the data assimilation system, *Q. J. R. Meteorol. Soc.*, 137(656), 553–597, doi:10.1002/qj.828, 2011.
- Deng, L., McCabe, M. F., Stenchikov, G., Evans, J. P. and Kucera, P. a.: Simulation of Flash-Flood-Producing Storm Events in Saudi Arabia Using the Weather Research and Forecasting Model, *J. Hydrometeorol.*, 16(2), 615–630, doi:10.1175/JHM-D-14-0126.1, 2015.
- Diomede, T., Marsigli, C., Montani, A., Nerozzi, F. and Paccagnella, T.: Calibration of limited-area ensemble precipitation forecasts for hydrological predictions, *Mon. Weather Rev.*, 142(6), 2176–2197, doi:10.1175/MWR-D-13-00071.1, 2014.
- Doswell, C. A., Brooks, H. E. and Maddox, R. A.: Flash Flood Forecasting: An Ingredients-Based Methodology, *Weather Forecast.*, 11(December 96), 560–581, doi:10.1175/1520-0434(1996)011<0560:FFFAIB>2.0.CO;2, 1996.
- Drobinski, P., Ducrocq, V., Alpert, P., Anagnostou, E., Béranger, K., Borga, M., Braud, I., Chanzy, A., Davolio, S., Delrieu, G., Estournel, C., Boubrahmi, N. F., Font, J., Grubišić, V., Gualdi, S., Homar, V., Ivančan-Picek, B., Kottmeier, C., Kotroni, V., Lagouvardos, K., Lionello, P., Llasat, M. C., Ludwig, W., Lutoff, C., Mariotti, A., Richard, E., Romero, R., Rotunno, R., Roussot, O., Ruin, I., Somot, S., Taupier-Letage, I., Tintore, J., Uijlenhoet, R. and Wernli, H.: HyMeX: A 10-Year
615 Multidisciplinary Program on the Mediterranean Water Cycle, *Bull. Am. Meteorol. Soc.*, 95(7), 1063–1082, doi:10.1175/BAMS-D-12-00242.1, 2014.
- Durrans, S. R., Julian, L. T. and Yekta, M.: Estimation of Depth-Area Relationships using Radar-Rainfall Data, *J. Hydrol. Eng.*, 7(5), 356–367, doi:10.1061/(ASCE)1084-0699(2002)7:5(356), 2002.
- Easterling, D. R., Evans, J. L., Groisman, P. Y., Karl, T. R., Kunkel, K. E. and Ambenje, P.: Observed variability and trends
620 in extreme climate events: A brief review, *Bull. Am. Meteorol. Soc.*, 81(3), 417–425, doi:10.1175/1520-0477(2000)081<0417:OVATIE>2.3.CO;2, 2000.
- El-Samra, R., Bou-Zeid, E. and El-Fadel, M.: To what extent does high-resolution dynamical downscaling improve the representation of climatic extremes over an orographically complex terrain?, *Theor. Appl. Climatol.*, doi:10.1007/s00704-017-2273-8, 2017.
- 625 Enzel, Y., Amit, R., Dayan, U., Crouvi, O., Kahana, R., Ziv, B. and Sharon, D.: The climatic and physiographic controls of the eastern Mediterranean over the late Pleistocene climates in the southern Levant and its neighboring deserts, *Glob. Planet. Change*, 60, 165–192, doi:10.1016/j.gloplacha.2007.02.003, 2008.
- Farhan, Y. and Anbar, A.: Fragile Landscape : Impact and Consequences of May 2014 Flash-flood Disaster in the Aqaba Area, Southern Jordan, *Res. J. Environ. Earth Sci.*, 6(9), 451–465, 2014.
- 630 Flaounas, E., Kotroni, V., Lagouvardos, K., Gray, S. L., Rysman, J. F. and Claud, C.: Heavy rainfall in Mediterranean cyclones. Part I: contribution of deep convection and warm conveyor belt, *Clim. Dyn.*, 50(7–8), 2935–2949, doi:10.1007/s00382-017-



- 3783-x, 2018.
- Flaounas, E., Fita, L., Lagouvardos, K. and Kotroni, V.: Heavy rainfall in Mediterranean cyclones, Part II: Water budget, precipitation efficiency and remote water sources, *Clim. Dyn.*, 0(0), 0, doi:10.1007/s00382-019-04639-x, 2019.
- 635 Fosser, G., Khodayar, S. and Berg, P.: Benefit of convection permitting climate model simulations in the representation of convective precipitation, *Clim. Dyn.*, 44(1–2), 45–60, doi:10.1007/s00382-014-2242-1, 2014.
- Gamo, M.: Thickness of the dry convection and large-scale subsidence above deserts, *Boundary-Layer Meteorol.*, 79(3), 265–278, doi:10.1007/BF00119441, 1996.
- Gehne, M., Hamill, T. M., Kiladis, G. N. and Trenberth, K. E.: Comparison of global precipitation estimates across a range of temporal and spatial scales, *J. Clim.*, 29(21), 7773–7795, doi:10.1175/JCLI-D-15-0618.1, 2016.
- 640 Gilleland, E., Ahijevych, D., Brown, B. G., Casati, B. and Ebert, E. E.: Intercomparison of Spatial Forecast Verification Methods, *Weather Forecast.*, 24(5), 1416–1430, doi:10.1175/2009WAF2222269.1, 2009.
- Giorgi, F. and Lionello, P.: Climate change projections for the Mediterranean region, *Glob. Planet. Change*, 63(2–3), 90–104, doi:10.1016/j.gloplacha.2007.09.005, 2008.
- 645 Goldreich, Y.: The spatial distribution of annual rainfall in Israel - a review, *Theor. Appl. Climatol.*, 50(1–2), 45–59, doi:10.1007/BF00864902, 1994.
- Goldreich, Y.: The climate of Israel: observation, research and application, Springer Science & Business Media., 2012.
- Goldreich, Y., Mozes, H. and Rosenfeld, D.: Radar analysis of cloud systems and their rainfall yield in Israel, *Isr. J. Earth Sci.*, 53(2), 63–76, doi:10.1560/G68K-30MN-D5V0-KUHU, 2004.
- 650 Gustafsson, N., Janjić, T., Schraff, C., Leuenberger, D., Weissmann, M., Reich, H., Brousseau, P., Montmerle, T., Wattrelot, E., Bučánek, A., Mile, M., Hamdi, R., Lindskog, M., Barkmeijer, J., Dahlbom, M., Macpherson, B., Ballard, S., Inverarity, G., Carley, J., Alexander, C., Dowell, D., Liu, S., Ikuta, Y. and Fujita, T.: Survey of data assimilation methods for convective-scale numerical weather prediction at operational centres, *Q. J. R. Meteorol. Soc.*, 144(713), 1218–1256, doi:10.1002/qj.3179, 2018.
- 655 Hahmann, A. N., Rostkier-Edelstein, D., Warner, T. T., Vandenberghe, F., Liu, Y., Babarsky, R. and Swerdlin, S. P.: A reanalysis system for the generation of mesoscale climatographies, *J. Appl. Meteorol. Climatol.*, 49(5), 954–972, doi:10.1175/2009JAMC2351.1, 2010.
- Hamill, T. M., Hagedorn, R. and Whitaker, J. S.: Probabilistic forecast calibration using ECMWF and GFS ensemble reforecasts. Part II: Precipitation, *Mon. Weather Rev.*, 136(7), 2620–2632, doi:10.1175/2007MWR2411.1, 2008.
- 660 Hersbach, H.: The ERA5 Atmospheric Reanalysis., AGU Fall Meet. Abstr., 2016.
- Hochman, A., Mercogliano, P., Alpert, P., Saaroni, H. and Bucchignani, E.: High-resolution projection of climate change and extremity over Israel using COSMO-CLM, *Int. J. Climatol.*, (January), 1–12, doi:10.1002/joc.5714, 2018a.
- Hochman, A., Harpaz, T., Saaroni, H. and Alpert, P.: The seasons' length in 21st century CMIP5 projections over the eastern Mediterranean, *Int. J. Climatol.*, (December 2017), 1–11, doi:10.1002/joc.5448, 2018b.
- 665 Hochman, A., Kunin, P., Alpert, P., Harpaz, T., Saaroni, H. and Rostkier-edelstein, D.: Statistical downscaling of seasonal



- precipitation over Israel for the 21st century, using CMIP5 projections, *Int. J. Climatol.*, in rev., 2019.
- Iacono, M. J., Delamere, J. S., Mlawer, E. J., Shephard, M. W., Clough, S. A. and Collins, W. D.: Radiative forcing by long-lived greenhouse gases: Calculations with the AER radiative transfer models, *J. Geophys. Res. Atmos.*, 113(D13), doi:10.1029/2008JD009944, 2008.
- 670 Israel, A. of: *The new Atlas of Israel: the national atlas*, Survey of Israel ; The Hebrew University of Jerusalem, Jerusalem., 2011.
- Ivatek-Šahdan, S., Stanešić, A., Tudor, M., Odak Plenković, I. and Janeković, I.: Impact of SST on heavy rainfall events on eastern Adriatic during SOP1 of HyMeX, *Atmos. Res.*, 200(September 2017), 36–59, doi:10.1016/j.atmosres.2017.09.019, 2018.
- 675 Janjić, Z. I.: The Step-Mountain Eta Coordinate Model: Further Developments of the Convection, Viscous Sublayer, and Turbulence Closure Schemes, *Mon. Weather Rev.*, 122(5), 927–945, doi:10.1175/1520-0493(1994)122<0927:TSMECM>2.0.CO;2, 1994.
- Kahana, R., Ziv, B., Enzel, Y. and Dayan, U.: Synoptic climatology of major floods in the Negev Desert, Israel, *Int. J. Climatol.*, 22(7), 867–882, doi:10.1002/joc.766, 2002.
- 680 Kalma, J. D. and Franks, S. W.: Rainfall in arid and semi-arid regions, in *Understanding Water in a Dry Environment*, edited by I. Simmers, pp. 15–64, Taylor & Francis., 2003.
- Karklinsky, M. and Morin, E.: Spatial characteristics of radar-derived convective rain cells over southern Israel, *Meteorol. Zeitschrift*, 15(5), 513–520, doi:10.1127/0941-2948/2006/0153, 2006.
- Keil, C., Heinlein, F. and Craig, G. C.: The convective adjustment time-scale as indicator of predictability of convective precipitation, *Q. J. R. Meteorol. Soc.*, 140(679), 480–490, doi:10.1002/qj.2143, 2014.
- 685 Kelley, C. P., Mohtadi, S., Cane, M. A., Seager, R. and Kushnir, Y.: Climate change in the Fertile Crescent and implications of the recent Syrian drought, *Proc. Natl. Acad. Sci.*, 112(11), 3241–3246, doi:10.1073/pnas.1421533112, 2015.
- Kendon, E. J., Roberts, N. M., Fowler, H. J., Roberts, M. J., Chan, S. C. and Senior, C. A.: Heavier summer downpours with climate change revealed by weather forecast resolution model, *Nat. Clim. Chang.*, 4(7), 570–576, doi:10.1038/nclimate2258, 2014.
- 690 Khodayar, S., Fossier, G., Berthou, S., Davolio, S., Drobinski, P., Ducrocq, V., Ferretti, R., Nuret, M., Pichelli, E., Richard, E. and Bock, O.: A seamless weather–climate multi-model intercomparison on the representation of a high impact weather event in the western Mediterranean: HyMeX IOP12, *Q. J. R. Meteorol. Soc.*, 142(April 2015), 433–452, doi:10.1002/qj.2700, 2016.
- Khodayar, S., Kalthoff, N. and Kottmeier, C.: Atmospheric conditions associated with heavy precipitation events in comparison to seasonal means in the western mediterranean region, *Clim. Dyn.*, 51(3), 951–967, doi:10.1007/s00382-016-3058-y, 2018.
- 695 Kidd, C., Becker, A., Huffman, G. J., Muller, C. L., Joe, P., Skofronick-Jackson, G. and Kirschbaum, D. B.: So, how much of the Earth’s surface is covered by rain gauges?, *Bull. Am. Meteorol. Soc.*, 98(1), 69–78, doi:10.1175/BAMS-D-14-00283.1, 2017.



- 700 Krichak, S. O., Alpert, P. and Krishnamurti, T. N.: Interaction of topography and tropospheric flow - A possible generator for the Red Sea Trough?, *Meteorol. Atmos. Phys.*, 63(3–4), 149–158, doi:10.1007/BF01027381, 1997.
- Krichak, S. O., Tsidulko, M. and Alpert, P.: November 2, 1994, severe storms in the southeastern Mediterranean, *Atmos. Res.*, 53(1–3), 45–62, doi:10.1016/S0169-8095(99)00045-9, 2000.
- Kushnir, Y., Dayan, U., Ziv, B., Morin, E. and Enzel, Y.: Climate of the Levant: phenomena and mechanisms, in *Quaternary of the Levant: environments, climate change, and humans*, edited by Y. Enzel and B.-Y. Ofer, pp. 31–44, Cambridge University Press, Cambridge, UK., 2017.
- 705 Maraun, D., Wetterhall, F., Chandler, R. E., Kendon, E. J., Widmann, M., Brienen, S., Rust, H. W., Sauter, T., Themeßl, M., Venema, V. K. C., Chun, K. P., Goodess, C. M., Jones, R. G., Onof, C., Vrac, M. and Thiele-Eich, I.: Precipitation downscaling under climate change: Recent developments to bridge the gap between dynamical models and the end user, *Rev. Geophys.*, 48(2009RG000314), 1–38, doi:10.1029/2009RG000314.1.INTRODUCTION, 2010.
- 710 Marra, F. and Morin, E.: Use of radar QPE for the derivation of Intensity–Duration–Frequency curves in a range of climatic regimes, *J. Hydrol.*, 531, 427–440, doi:10.1016/j.jhydrol.2015.08.064, 2015.
- Marra, F. and Morin, E.: Autocorrelation structure of convective rainfall in semiarid-arid climate derived from high-resolution X-Band radar estimates, *Atmos. Res.*, 200(September 2017), 126–138, doi:10.1016/j.atmosres.2017.09.020, 2018.
- 715 Marra, F., Morin, E., Peleg, N., Mei, Y. and Anagnostou, E. N.: Intensity-duration-frequency curves from remote sensing rainfall estimates: comparing satellite and weather radar over the eastern Mediterranean, *Hydrol. Earth Syst. Sci.*, 21(5), 2389–2404, doi:10.5194/hess-21-2389-2017, 2017.
- Marra, F., Zoccatelli, D., Armon, M. and Morin, E.: A simplified MEV formulation to model extremes emerging from multiple nonstationary underlying processes, *Adv. Water Resour.*, 127(March), 280–290, doi:10.1016/j.advwatres.2019.04.002, 2019.
- 720 Marsham, J. H., Hobby, M., Allen, C. J. T., Banks, J. R., Bart, M., Brooks, B. J., Cavazos-Guerra, C., Engelstaedter, S., Gascoyne, M., Lima, A. R., Martins, J. V., McQuaid, J. B., O’Leary, A., Ouchene, B., Ouladichir, A., Parker, D. J., Saci, A., Salah-Ferroudj, M., Todd, M. C. and Washington, R.: Meteorology and dust in the central Sahara: Observations from Fennec supersite-1 during the June 2011 Intensive Observation Period, *J. Geophys. Res. Atmos.*, 118(10), 4069–4089, doi:10.1002/jgrd.50211, 2013.
- 725 Mass, C. F., Ovens, D., Westrick, K. and Colle, B. A.: Does Increasing Horizontal Resolution Produce More Skillful Forecasts?, *Bull. Am. Meteorol. Soc.*, 83(3), 407–430, doi:10.1175/1520-0477(2002)083<0407:DIHRPM>2.3.CO;2, 2002.
- Merz, R. and Blöschl, G.: A process typology of regional floods, *Water Resour. Res.*, 39(12), 1–20, doi:10.1029/2002WR001952, 2003.
- Morin, E. and Gabella, M.: Radar-based quantitative precipitation estimation over Mediterranean and dry climate regimes, *J. Geophys. Res.*, 112(D20), D20108, doi:10.1029/2006JD008206, 2007.
- 730 Morin, E., Krajewski, W. F., Goodrich, D. C., Gao, X. and Sorooshian, S.: Estimating Rainfall Intensities from Weather Radar Data: The Scale-Dependency Problem, *J. Hydrometeorol.*, 4(5), 782–797, doi:10.1175/1525-7541(2003)004<0782:ERIFWR>2.0.CO;2, 2003.



- Morin, E., Harats, N., Jacoby, Y., Arbel, S., Getker, M., Arazi, A., Grodek, T., Ziv, B. and Dayan, U.: Studying the extremes: hydrometeorological investigation of a flood-causing rainstorm over Israel, *Adv. Geosci.*, 12, 107–114, doi:10.5194/adgeo-12-107-2007, 2007.
- Morin, E., Jacoby, Y., Navon, S. and Bet-Halachmi, E.: Towards flash-flood prediction in the dry Dead Sea region utilizing radar rainfall information, *Adv. Water Resour.*, 32(7), 1066–1076, doi:10.1016/j.advwatres.2008.11.011, 2009.
- Morin, E., Marra, F. and Armon, M.: Dryland Precipitation Climatology from Satellite Observations, in *Satellite Precipitation Measurement*, edited by V. Levizzani, C. Kidd, D. Kirschbaum, C. Kummerow, and F. J. Turk, Springer., 2019.
- Nasta, P., Adane, Z., Lock, N., Houston, A. and Gates, J. B.: Links between episodic groundwater recharge rates and rainfall events classified according to stratiform-convective storm scoring: A plot-scale study in eastern Nebraska, *Agric. For. Meteorol.*, 259(February), 154–161, doi:10.1016/j.agrformet.2018.05.003, 2018.
- Nerini, D., Besic, N., Sideris, I., Germann, U. and Foresti, L.: A non-stationary stochastic ensemble generator for radar rainfall fields based on the short-space Fourier transform, *Hydrol. Earth Syst. Sci.*, 21(6), 2777–2797, doi:10.5194/hess-21-2777-2017, 2017.
- Nicholson, S. E.: *Dryland climatology*, Cambridge University Press, New York., 2011.
- Nuissier, O., Joly, B., Joly, A., Ducrocq, V. and Arbogast, P.: A statistical downscaling to identify the large-scale circulation patterns associated with heavy precipitation events over southern France, *Q. J. R. Meteorol. Soc.*, 137(660), 1812–1827, doi:10.1002/qj.866, 2011.
- Panziera, L., James, C. N. and Germann, U.: Mesoscale organization and structure of orographic precipitation producing flash floods in the Lago Maggiore region, *Q. J. R. Meteorol. Soc.*, 141(686), 224–248, doi:10.1002/qj.2351, 2015.
- Panziera, L., Gabella, M., Germann, U. and Martius, O.: A 12-year radar-based climatology of daily and sub-daily extreme precipitation over the Swiss Alps, *Int. J. Climatol.*, 38(10), 3749–3769, doi:10.1002/joc.5528, 2018.
- Pastor, F., Estrela, M. J., Peñarrocha, D. and Millán, M. M.: Torrential Rains on the Spanish Mediterranean Coast: Modeling the Effects of the Sea Surface Temperature, *J. Appl. Meteorol.*, 40(7), 1180–1195, doi:10.1175/1520-0450(2001)040<1180:trotsm>2.0.co;2, 2002.
- Peleg, N. and Morin, E.: Convective rain cells: Radar-derived spatiotemporal characteristics and synoptic patterns over the eastern Mediterranean, *J. Geophys. Res. Atmos.*, 117(15), 1–17, doi:10.1029/2011JD017353, 2012.
- Peleg, N., Morin, E., Gvirtzman, H. and Enzel, Y.: Rainfall, spring discharge and past human occupancy in the Eastern Mediterranean, *Clim. Change*, 112(3–4), 769–789, doi:10.1007/s10584-011-0232-4, 2012.
- Peleg, N., Marra, F., Fatichi, S., Molnar, P., Morin, E., Sharma, A. and Burlando, P.: Intensification of convective rain cells at warmer temperatures observed from high-resolution weather radar data, *J. Hydrometeorol.*, JHM-D-17-0158.1, doi:10.1175/JHM-D-17-0158.1, 2018.
- Prein, A. F., Langhans, W., Fosser, G., Ferrone, A., Ban, N., Goergen, K., Keller, M., Tölle, M., Gutjahr, O., Feser, F., Brisson, E., Kollet, S., Schmidli, J., Van Lipzig, N. P. M. and Leung, R.: A review on regional convection-permitting climate modeling: Demonstrations, prospects, and challenges, *Rev. Geophys.*, 53(2), 323–361, doi:10.1002/2014RG000475, 2015.



- Raveh-Rubin, S. and Wernli, H.: Large-scale wind and precipitation extremes in the Mediterranean: a climatological analysis for 1979–2012, *Q. J. R. Meteorol. Soc.*, (June 2013), n/a–n/a, doi:10.1002/qj.2531, 2015.
- 770 Rinat, Y., Marra, F., Zoccatelli, D. and Morin, E.: Controls of flash flood peak discharge in Mediterranean basins and the special role of runoff-contributing areas, *J. Hydrol.*, 565(April), 846–860, doi:10.1016/j.jhydrol.2018.08.055, 2018.
- Roberts, N. M. and Lean, H. W.: Scale-Selective Verification of Rainfall Accumulations from High-Resolution Forecasts of Convective Events, *Mon. Weather Rev.*, 136(1), 78–97, doi:10.1175/2007MWR2123.1, 2008.
- Romine, G. S., Schwartz, C. S., Snyder, C., Anderson, J. L. and Weisman, M. L.: Model Bias in a Continuously Cycled
775 Assimilation System and Its Influence on Convection-Permitting Forecasts, *Mon. Weather Rev.*, 141(4), 1263–1284, doi:10.1175/MWR-D-12-00112.1, 2013.
- Rostkier-edelstein, D., Kunin, P., Hopson, T. M. and Givati, A.: Statistical downscaling of seasonal precipitation in Israel, *Int. J. Climatol.*, doi:10.1002/joc.4368, 2015.
- Rostkier-Edelstein, D., Liu, Y., Wu, W., Kunin, P., Givati, A. and Ge, M.: Towards a high-resolution climatology of seasonal
780 precipitation over Israel, *Int. J. Climatol.*, 34(6), 1964–1979, doi:10.1002/joc.3814, 2014.
- Rubin, S., Ziv, B. and Paldor, N.: Tropical Plumes over Eastern North Africa as a Source of Rain in the Middle East, *Mon. Weather Rev.*, 135(12), 4135–4148, doi:10.1175/2007MWR1919.1, 2007.
- Saaroni, H., Halfon, N., Ziv, B., Alpert, P. and Kutiel, H.: Links between the rainfall regime in Israel and location and intensity of Cyprus lows, *Int. J. Climatol.*, 30(7), 1014–1025, doi:10.1002/joc.1912, 2010.
- 785 Saaroni, H., Ziv, B., Lempert, J., Gazit, Y. and Morin, E.: Prolonged dry spells in the Levant region: Climatologic-synoptic analysis, *Int. J. Climatol.*, 2236(September 2014), 2223–2236, doi:10.1002/joc.4143, 2014.
- Saltikoff, E., Friedrich, K., Soderholm, J., Lengfeld, K., Nelson, B., Becker, A., Hollmann, R., Urban, B., Heistermann, M. and Tassone, C.: An overview of using weather radar for climatological studies: Successes, challenges and potential., *Bull. Am. Meteorol. Soc.*, doi:10.1175/bams-d-18-0166.1, 2019.
- 790 Samuels, R., Rimmer, A. and Alpert, P.: Effect of extreme rainfall events on the water resources of the Jordan River, *J. Hydrol.*, 375(3–4), 513–523, doi:10.1016/j.jhydrol.2009.07.001, 2009.
- Schär, C., Ban, N., Fischer, E. M., Rajczak, J., Schmidli, J., Frei, C., Giorgi, F., Karl, T. R., Kendon, E. J., Tank, A. M. G. K., O’Gorman, P. A., Sillmann, J., Zhang, X. and Zwiers, F. W.: Percentile indices for assessing changes in heavy precipitation events, *Clim. Change*, 137(1–2), 201–216, doi:10.1007/s10584-016-1669-2, 2016.
- 795 Schick, A. P.: Hydrologic aspects of floods in extreme arid environments, in *Flood geomorphology*, edited by V. R. Baker, R. C. Kochel, and P. C. Patton, pp. 189–203, John Wiley and Sons, New York., 1988.
- Schwartz, C. S., Romine, G. S., Sobash, R. A., Fossell, K. R. and Weisman, M. L.: NCAR’s Experimental Real-Time Convection-Allowing Ensemble Prediction System, *Weather Forecast.*, 30(6), 1645–1654, doi:10.1175/WAF-D-15-0103.1, 2015.
- 800 Seager, R., Liu, H., Henderson, N., Simpson, I., Kelley, C., Shaw, T., Kushnir, Y. and Ting, M.: Causes of increasing aridification of the mediterranean region in response to rising greenhouse gases, *J. Clim.*, 27(12), 4655–4676,



- doi:10.1175/JCLI-D-13-00446.1, 2014.
- Sharon, D.: The spottiness of rainfall in a desert area, *J. Hydrol.*, 17(3), 161–175, doi:10.1016/0022-1694(72)90002-9, 1972.
- Sharon, D. and Kutiel, H.: The distribution of rainfall intensity in Israel, its regional and seasonal variations and its climatological evaluation, *J. Climatol.*, 6(3), 277–291, doi:10.1002/joc.3370060304, 1986.
- 805 Skamarock, W. C., Klemp, J. B., Dudhia, J., Gill, D. O., Barker, D. M., Duda, M. G., Huang, X. Y., Wang, W. and Powers, J. G.: A Description of the Advanced Research WRF Version 3, , 113, doi:10.5065/D68S4MVH, 2008.
- Smith, J. a., Baeck, M. L., Zhang, Y. and Doswell, C. a.: Extreme Rainfall and Flooding from Supercell Thunderstorms, *J. Hydrometeorol.*, 2(5), 469–489, doi:10.1175/1525-7541(2001)002<0469:ERAFFS>2.0.CO;2, 2001.
- 810 Smith, J. A., Baeck, M. L., Villarini, G., Welty, C., Miller, A. J. and Krajewski, W. F.: Analyses of a long-term, high-resolution radar rainfall data set for the Baltimore metropolitan region, *Water Resour. Res.*, 48(4), 1–14, doi:10.1029/2011WR010641, 2012.
- Sowers, J., Vengosh, A. and Weinthal, E.: Climate change, water resources, and the politics of adaptation in the Middle East and North Africa, *Clim. Change*, 104(3–4), 599–627, doi:10.1007/s10584-010-9835-4, 2010.
- 815 Tarolli, P., Borga, M., Morin, E. and Delrieu, G.: Analysis of flash flood regimes in the North-Western and South-Eastern Mediterranean regions, *Nat. Hazards Earth Syst. Sci.*, 12(5), 1255–1265, doi:10.5194/nhess-12-1255-2012, 2012.
- Taylor, R. G., Todd, M. C., Kongola, L., Maurice, L., Nahozya, E., Sanga, H. and Macdonald, A. M.: Evidence of the dependence of groundwater resources on extreme rainfall in East Africa, *Nat. Clim. Chang.*, 3(4), 374–378, doi:10.1038/nclimate1731, 2013.
- 820 Tewari, M., Chen, F., Wang, W., Dudhia, J., LeMone, M. A., Mitchell, K., Ek, M., Gayno, G., Wegiel, J. and Cuenca, R. H.: Implementation and verification of the unified NOAA land surface model in the WRF model (Formerly Paper Number 17.5), in 20th Conference on Weather Analysis and Forecasting/16th Conference on Numerical Weather Prediction, pp. 11–15., 2004.
- Thompson, G., Field, P. R., Rasmussen, R. M. and Hall, W. D.: Explicit Forecasts of Winter Precipitation Using an Improved Bulk Microphysics Scheme. Part II: Implementation of a New Snow Parameterization, *Mon. Weather Rev.*, 136(12), 5095–5115, doi:10.1175/2008MWR2387.1, 2008.
- 825 Thorndahl, S., Smith, J. A., Baeck, M. L. and Krajewski, W. F.: Analyses of the temporal and spatial structures of heavy rainfall from a catalog of high-resolution radar rainfall fields, *Atmos. Res.*, 144, 111–125, doi:10.1016/j.atmosres.2014.03.013, 2014.
- Tiedtke, M.: A Comprehensive Mass Flux Scheme for Cumulus Parameterization in Large-Scale Models, *Mon. Weather Rev.*, 117(8), 1779–1800, doi:10.1175/1520-0493(1989)117<1779:ACMFSF>2.0.CO;2, 1989.
- 830 Trenberth, K. E., Dai, A., Rasmussen, R. M. and Parsons, D. B.: The changing character of precipitation, *Bull. Am. Meteorol. Soc.*, 84(9), 1205–1217+1161, doi:10.1175/BAMS-84-9-1205, 2003.
- Tubi, A., Dayan, U. and Lensky, I. M.: Moisture transport by tropical plumes over the Middle East: a 30-year climatology, *Q. J. R. Meteorol. Soc.*, 143(709), 3165–3176, doi:10.1002/qj.3170, 2017.
- 835 UN-Habitat: Cities and Climate Change: Global Report on Human Settlements 2011, Earthscan, London & Washington, DC.



- [online] Available from:
<http://books.google.com/books?hl=en&lr=&id=GZG5x6SbeSAC&oi=fnd&pg=PA91&dq=Cities+and+Climate+Change&ots=adeiArrg6X&sig=9TeIo2HeRHPqS1KwBKsvkC78Afg> (Accessed 3 January 2015), 2011.
- Villarini, G., Mandapaka, P. V., Krajewski, W. F. and Moore, R. J.: Rainfall and sampling uncertainties: A rain gauge
840 perspective, *J. Geophys. Res. Atmos.*, 113(11), 1–12, doi:10.1029/2007JD009214, 2008.
- Vincendon, B., Ducrocq, V., Nuissier, O. and Vié, B.: Perturbation of convection-permitting NWP forecasts for flash-flood ensemble forecasting, *Nat. Hazards Earth Syst. Sci.*, 11(5), 1529–1544, doi:10.5194/nhess-11-1529-2011, 2011.
- De Vries, A. J., Tyrlis, E., Edry, D., Krichak, S. O., Steil, B. and Lelieveld, J.: Extreme precipitation events in the Middle East: Dynamics of the Active Red Sea Trough, *J. Geophys. Res. Atmos.*, 118(13), 7087–7108, doi:10.1002/jgrd.50569, 2013.
- 845 Warner, T. T.: *Desert Meteorology*, Cambridge University Press, New York., 2004.
- Warner, T. T.: *Numerical Weather and Climate Prediction.*, 2011.
- Wernli, H., Paulat, M., Hagen, M. and Frei, C.: SAL—A Novel Quality Measure for the Verification of Quantitative Precipitation Forecasts, *Mon. Weather Rev.*, 136(11), 4470–4487, doi:10.1175/2008MWR2415.1, 2008.
- Wernli, H., Hofmann, C. and Zimmer, M.: Spatial Forecast Verification Methods Intercomparison Project: Application of the
850 SAL Technique, *Weather Forecast.*, 24(6), 1472–1484, doi:10.1175/2009WAF2222271.1, 2009.
- Westra, S., Fowler, H. J., Evans, J. P., Alexander, L. V., Berg, P., Johnson, F., Kendon, E. J., Lenderink, G. and Roberts, N. M.: Future changes to the intensity and frequency of short-duration extreme rainfall, *Rev. Geophys.*, 52, 522–555, doi:10.1002/2014RG000464, 2014.
- Yang, L., Smith, J. A., Baeck, M. L., Bou-Zeid, E., Jessup, S. M., Tian, F. and Hu, H.: Impact of Urbanization on Heavy
855 Convective Precipitation under Strong Large-Scale Forcing: A Case Study over the Milwaukee–Lake Michigan Region, *J. Hydrometeorol.*, 15(1), 261–278, doi:10.1175/JHM-D-13-020.1, 2014.
- Yano, J. I. I., Ziemian´ski, Mi. Z., Cullen, Mi., Termonia, Pi., Onvlee, J., Bengtsson, L., Carrassi, A., Davy, R., Deluca, A., Gray, S. L., Homar, V., Köhler, M. I., Krichak, S., Michaelides, S., Phillips, V. T. J., Soares, P. M. M. and Wyszogrodzki, A. A.: Scientific challenges of convective-scale numerical weather prediction, *Bull. Am. Meteorol. Soc.*, 99(4), 699–710,
860 doi:10.1175/BAMS-D-17-0125.1, 2018.
- Zepeda-Arce, J., Foufoula-Georgiou, E. and Droegemeier, K. K.: Space-time rainfall organization and its role in validating quantitative precipitation forecasts, *J. Geophys. Res. Atmos.*, 105(D8), 10129–10146, doi:10.1029/1999JD901087, 2000.
- Zhang, C., Wang, Y. and Hamilton, K.: Improved Representation of Boundary Layer Clouds over the Southeast Pacific in ARW-WRF Using a Modified Tiedtke Cumulus Parameterization Scheme, *Mon. Weather Rev.*, 139(11), 3489–3513,
865 doi:10.1175/MWR-D-10-05091.1, 2011a.
- Zhang, F., Bei, N., Rotunno, R., Snyder, C. and Epifanio, C. C.: Mesoscale Predictability of Moist Baroclinic Waves: Convection-Permitting Experiments and Multistage Error Growth Dynamics, *J. Atmos. Sci.*, 64(10), 3579–3594, doi:10.1175/JAS4028.1, 2007.
- Zhang, X., Alexander, L., Hegerl, G. C., Jones, P., Tank, A. K., Peterson, T. C., Trewin, B. and Zwiers, F. W.: Indices for

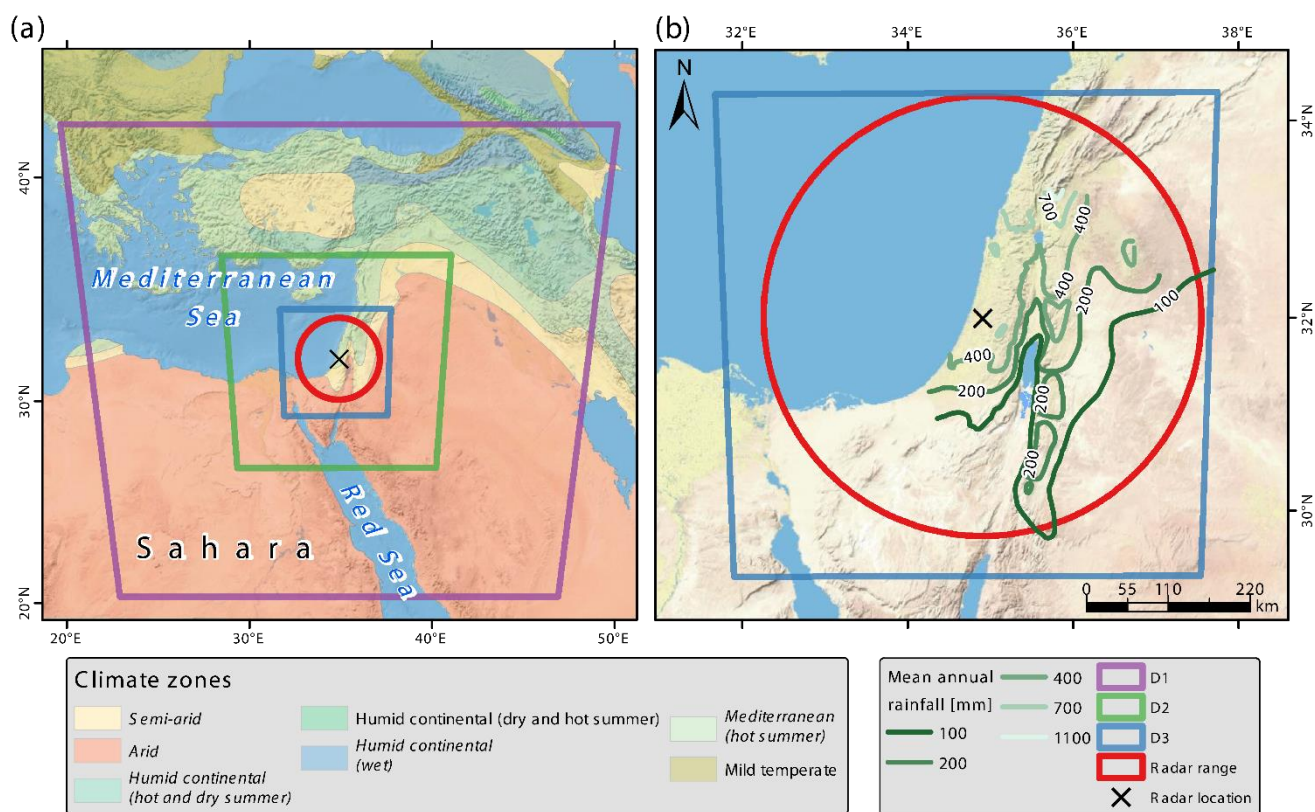


870 monitoring changes in extremes based on daily temperature and precipitation data, Wiley Interdiscip. Rev. Clim. Chang., 2(6),
 851–870, doi:10.1002/wcc.147, 2011b.

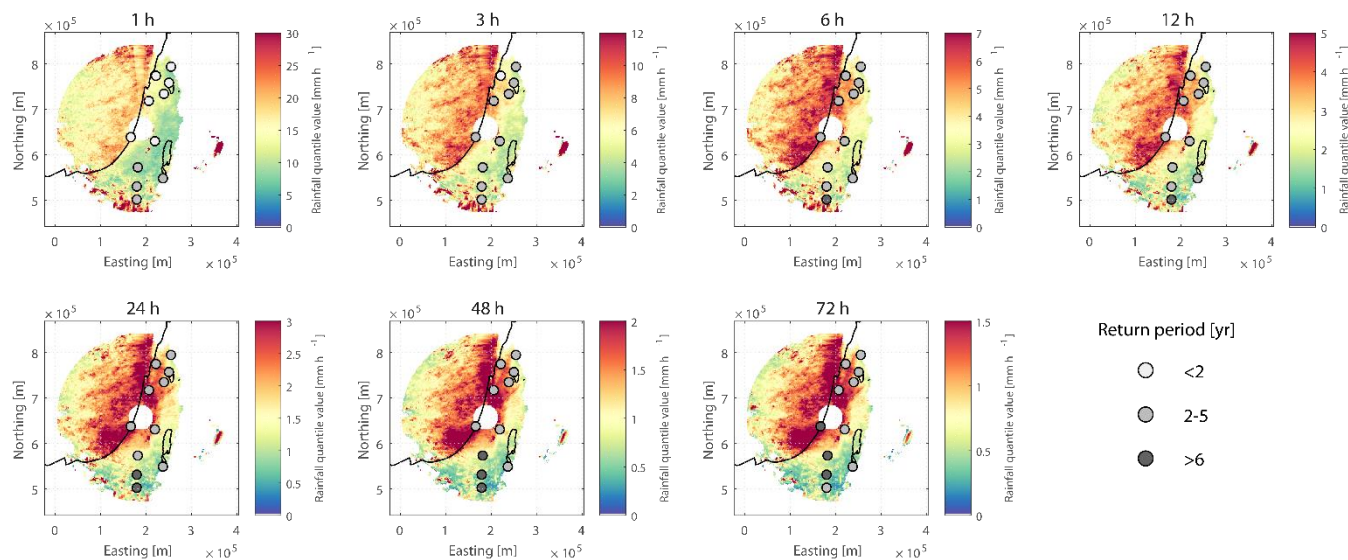
Ziv, B., Harpaz, T., Saaroni, H. and Blender, R.: A new methodology for identifying daughter cyclogenesis: application for
 the Mediterranean Basin, Int. J. Climatol., n/a-n/a, doi:10.1002/joc.4250, 2015.

Zoccatelli, D., Marra, F., Armon, M., Rinat, Y., Smith, J. A. and Morin, E.: Contrasting rainfall-runoff characteristics of floods
 875 in Desert and Mediterranean basins, Hydrol. Earth Syst. Sci. Discuss., 12, 2665–2678, doi:https://doi.org/10.5194/hess-23-
 2665-2019, 2019.

Figures and tables

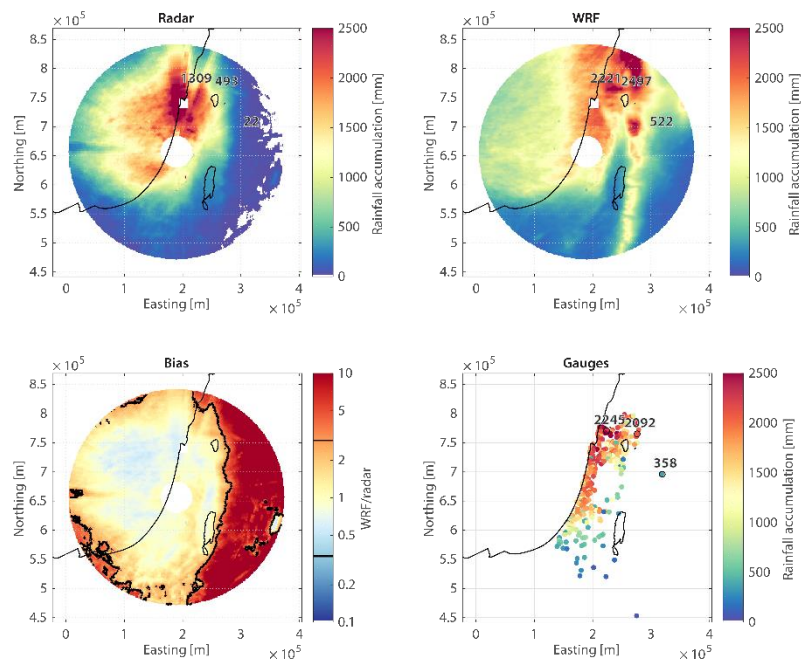


880 **Figure 1: Study region.** (a) climate zones in the eastern Mediterranean, three nested domains used in the weather model (D1-3; purple, green and blue) and the radar domain (red). (b) mean annual rainfall isohyets, radar and innermost model domains. Climatic classification is from the Atlas of Israel (2011). Basemap source: U.S. National Park Service.



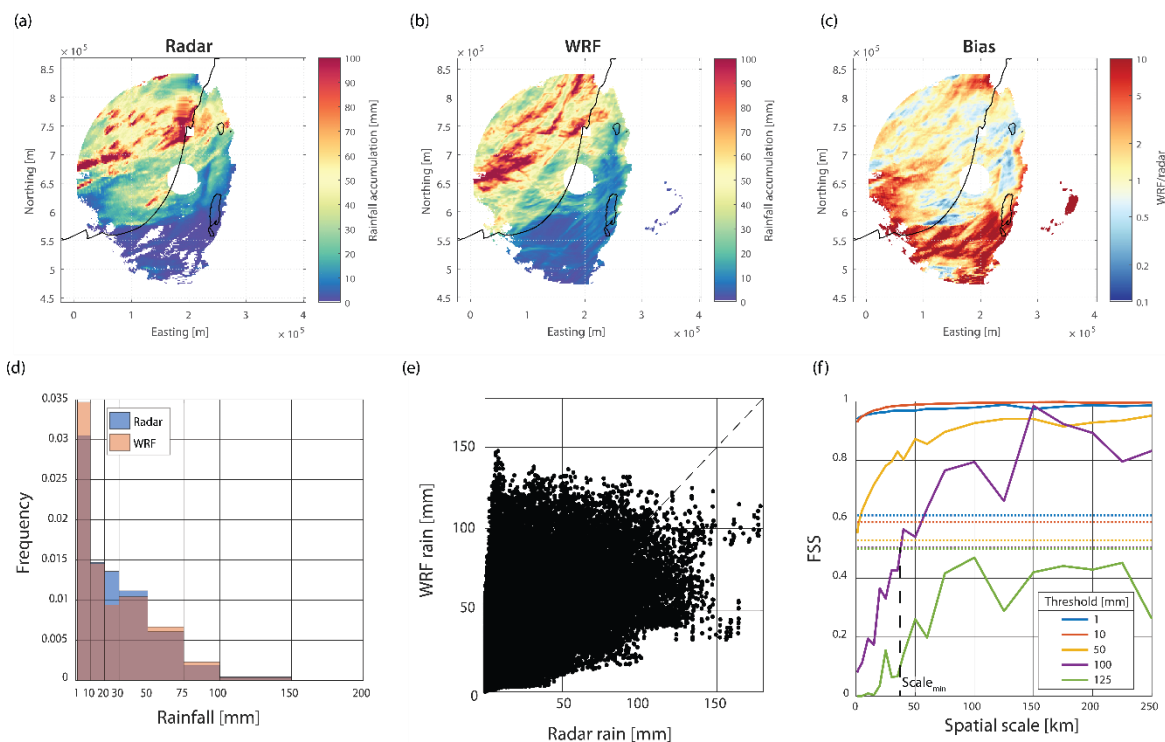
885 **Figure 2: The 99.5% rain intensity quantile of each radar pixel for durations of 1 h (top-left) to 72 h (bottom-right). Notice change in colour scale between different durations. Also shown are annual return periods of the rain intensity threshold averaged over nine pixels around 11 locations (generalised extreme value fit of the rain gauge annual maxima series, using the method of the probability weighted moments, with records of at least 44-year). These computed annual return periods range between 1.8 and 10.4 yr.**

890





895 **Figure 3: Total cumulative rainfall for all 41 HPEs, from (a) radar-derived QPE, (b) WRF-derived rainfall, and (d) daily rain gauges. (c) WRF to radar rainfall accumulation ratio (logarithmic colour scale). The 3 and 1/3 bias region is marked in black. Highlighted in (d) are total accumulations [mm] measured at three rain gauges from regions where radar-QPE is considered to be inferior; corresponding radar and WRF, 9-pixel averaged values [mm] centred over the same locations, are shown in (a) and (b), respectively.**



900 **Figure 4: HPE #1 (02-Nov-1991 09:00 - 05-Nov-1991 09:00 [Local winter time]; see Table S1). Cumulative rainfall from (a) radar-**
 905 **derived QPE, (b) WRF-derived rainfall, and their ratio (c; logarithmic colour scale). A pixel-based comparison between rainfall accumulations using a histogram (d; zero rainfall is omitted) and scatter plot (e). Notice that although rainfall distribution is quite well represented (d), results of a single pixel might deviate substantially from the 1:1 line (e; dashed). The fractions skill score (FSS) for the same event for various cumulative rainfall thresholds is presented in panel (f). Dashed lines are uniform FSS for the same rainfall thresholds. Also shown (dashed black line) is the minimal scale for a valuable prediction for a 100 mm rain depth (at the crossing of the FSS and the uniform FSS; see details in supplementary material [S1]).**

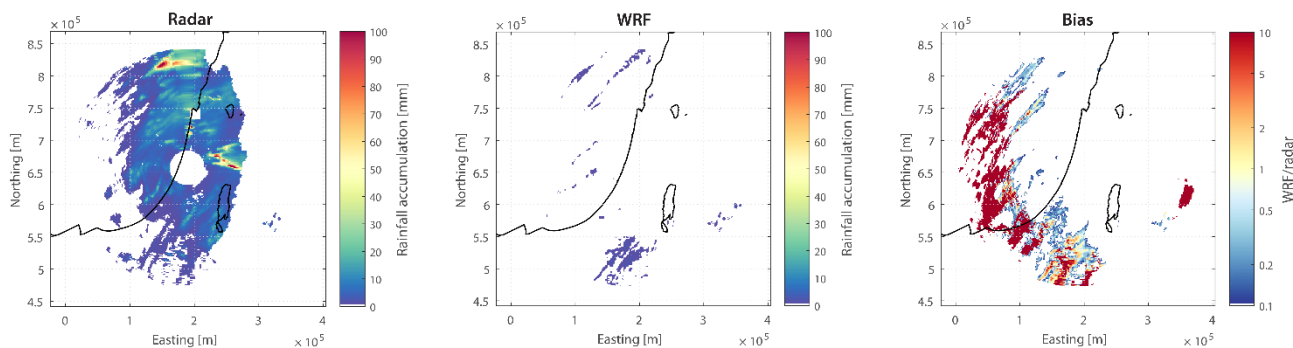
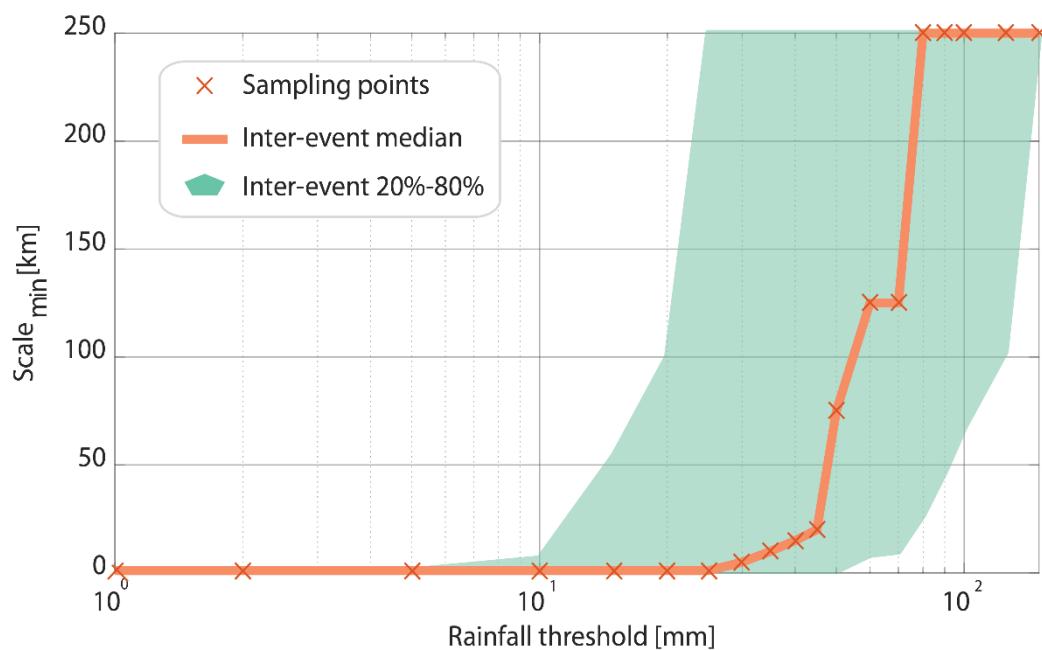
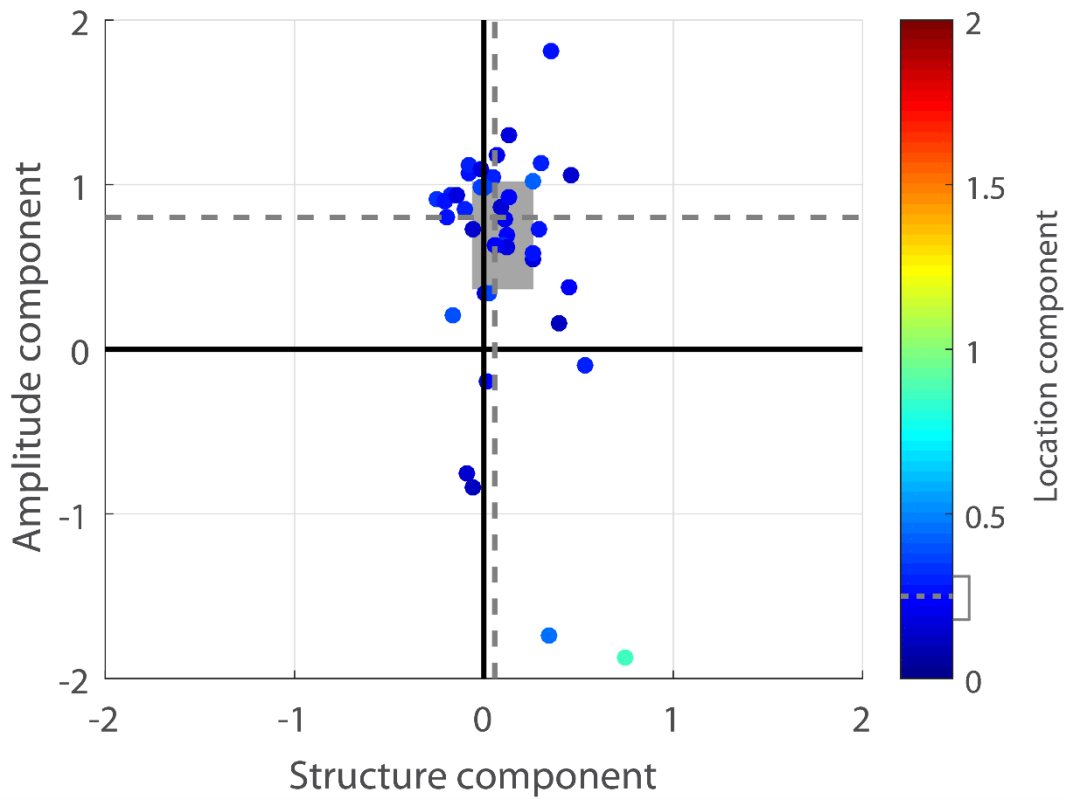


Figure 5: Same as Fig. 4 a-c, for HPE #5 (31-Mar-1993 09:00 - 02-Apr-1993 02:00; Table S1).

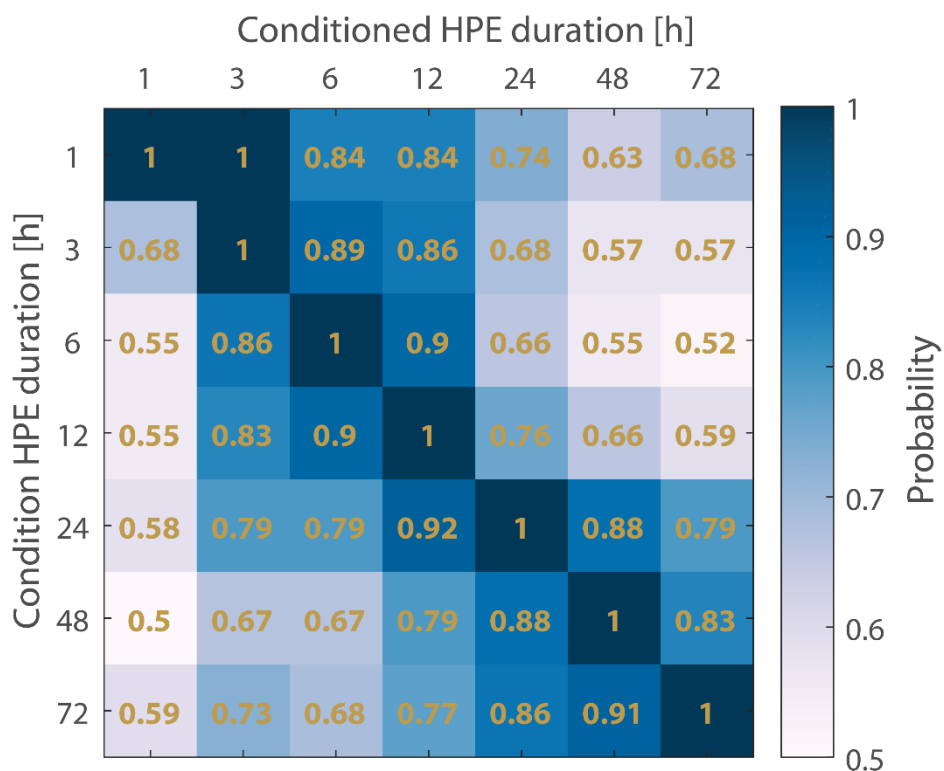


910

Figure 6: Minimal scale (see Fig. 4f and supplementary material [S1]) derived for all 41 events for various rainfall thresholds.



915 **Figure 7: Structure-Amplitude-Location (SAL) analysis (Wernli et al., 2008). Each dot represents one event. Dashed lines are median values and the grey rectangles represent the 25th – 75th percentile ranges. Location component median value is 0.25, and its 25th – 75th range is 0.18-0.31. More details are in the supplementary material (S2).**



920 **Figure 8: Probability of a HPE with a given duration listed on the x-axis conditioned on being a HPE with a duration listed on the y-axis.**

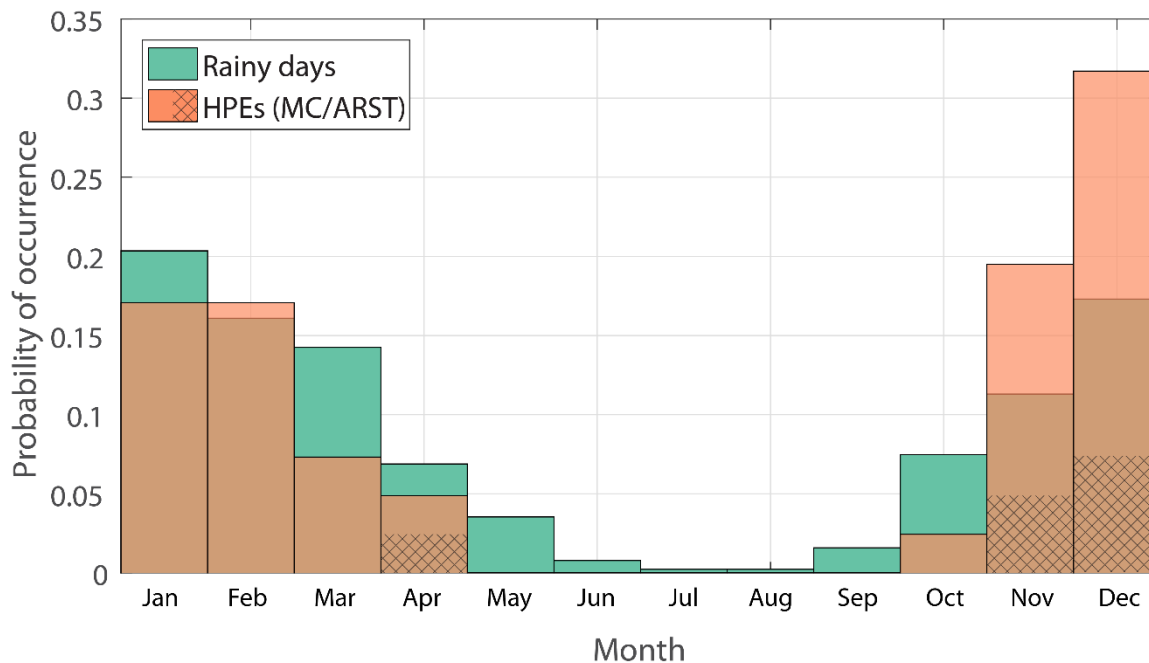


Figure 9: Monthly probability of occurrence of rainy days near the radar location (green; Bet-Dagan rain gauge, 32.0°N, 34.8°E), and of HPEs from the radar archive (orange). Hatching represents HPEs classified as ARST.

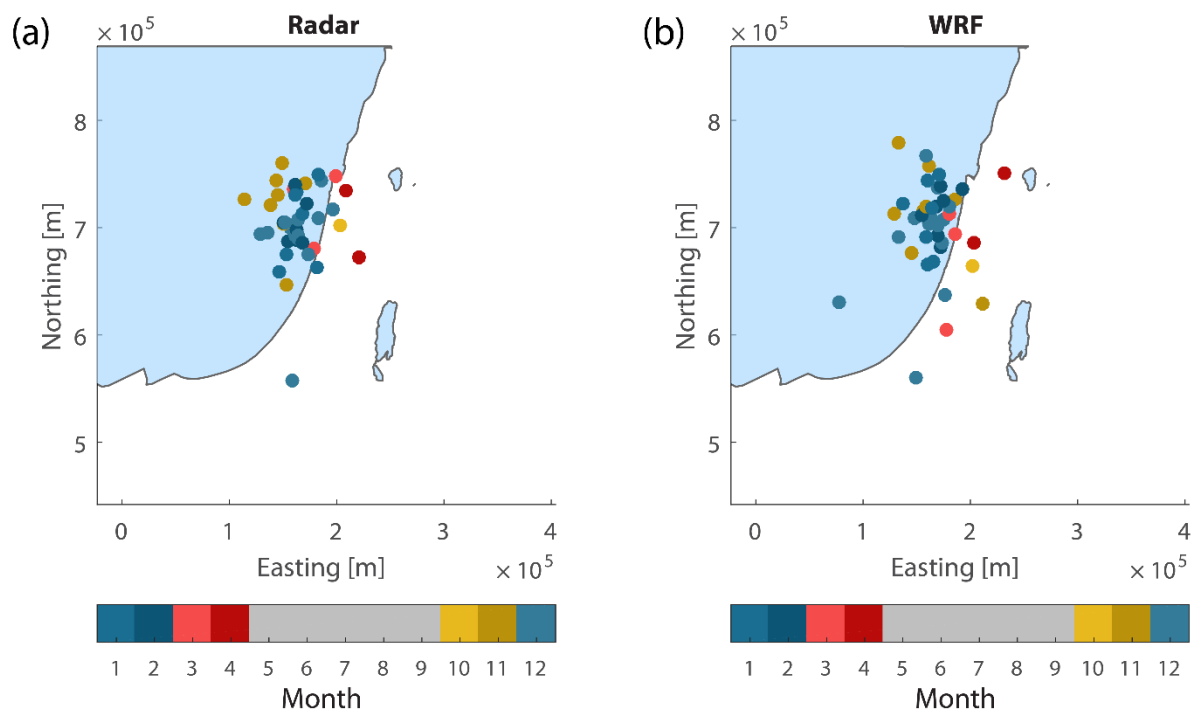


Figure 10: Centres of mass of cumulative rainfall of all HPEs derived from (a) radar QPE and (b) WRF. Colours represent month of occurrence.

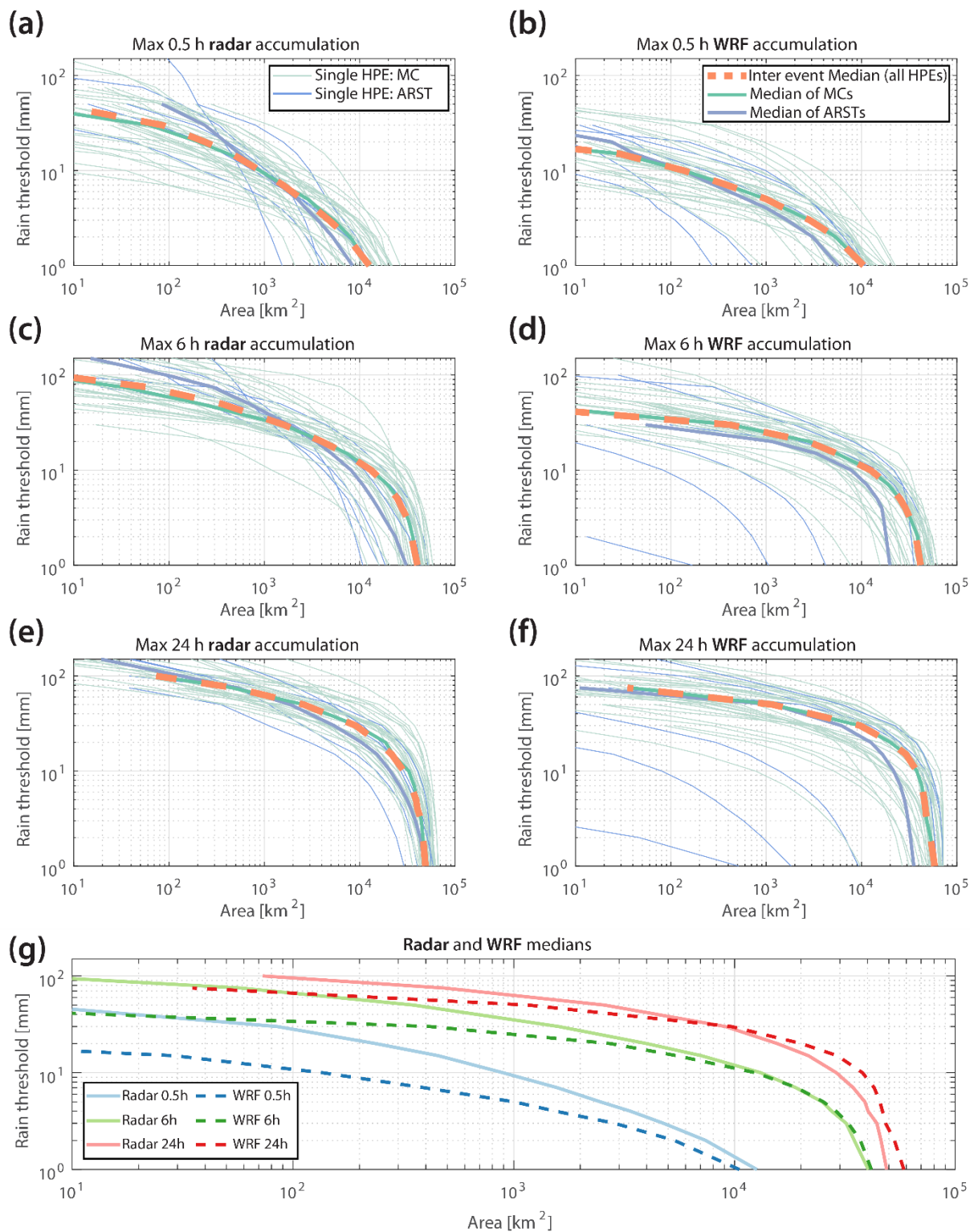




Figure 11: Depth-Area-Duration (DAD) curves showing the maximal amount of rainfall as a function of area, derived from the radar (left; a, c and e) and from the WRF model (right; b, d and f) for 0.5 h (top), 6 h (middle) and 24 h (bottom). Green and purple lines represent HPEs classified as MCs and ARSTs, respectively. Thick lines represent the inter-event median. This median is compared between radar-QPE and WRF rainfall in panel g.

935

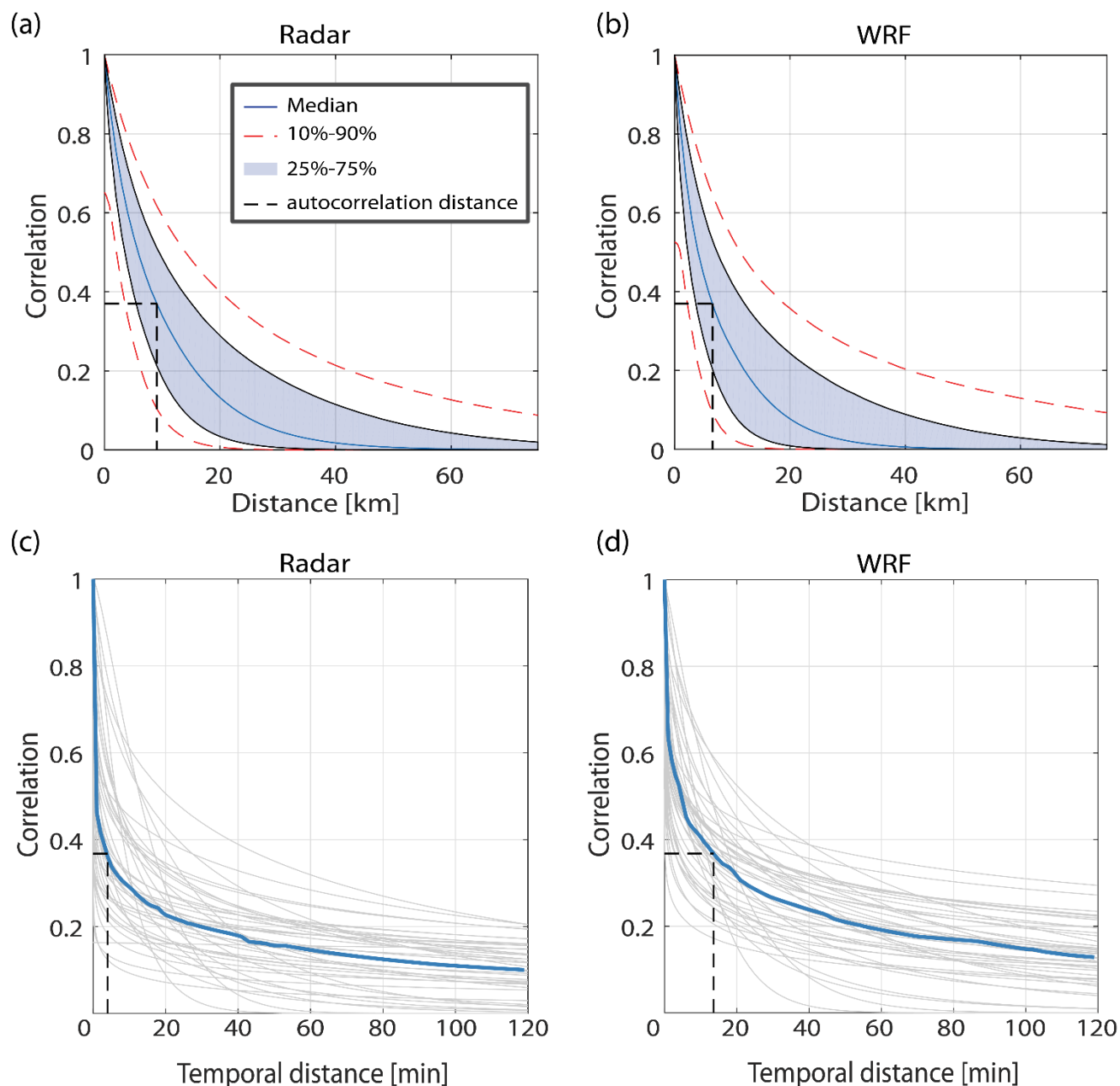


Figure 12: 1-D exponential fitting of rain field spatial (a, b) and temporal (c, d) autocorrelation values from radar-derived QPE (a, c) and from the WRF model (b, d). These were computed using 10 min snapshots of rain and only for periods where convective



940 rainfall is present. Quantiles in spatial autocorrelation (a, b) represent 11731 snapshots of radar 10 min data, and 14323 WRF rainfall snapshots. Temporal autocorrelation plots (c, d) are composed of the 41 examined HPEs (grey), and their median values (blue).

	Outer nest	Middle nest	Inner nest
Domains			
Spatial resolution [km]	25X25	5X5	1X1
Temporal resolution [s]	~100	~20	4-8
Domain size [pixels]	100X100	221X221	551X551
Number of vertical layers	68	68	68
Model top [hPa]	25	25	25
Physics			
Cumulus scheme	Tiedtke (Tiedtke, 1989; Zhang et al., 2011a)		-
Microphysical scheme	Thompson (Thompson et al., 2008)		
Radiative transfer scheme	RRTMG Shortwave and Longwave (Iacono et al., 2008)		
Planetary boundary layer scheme	Mellor–Yamada– Janjić (Janjić, 1994)		
Surface layer scheme	Eta Similarity Scheme (Janjić, 1994)		
Land surface model	Unified Noah Land Surface (Tewari et al., 2004)		

Table 1: WRF Model settings and specifications